**Universidade de Aveiro** Departamento de Química
**Ano 2010**

**Rita Paula Paiva Craveiro**

# Desenvolvimento de Novos Materiais Microporosos

# Developing Novel Microporous Materials

**Universidade de Aveiro** Departamento de Química
**Ano 2010**

**Rita Paula Paiva Craveiro**

# Desenvolvimento de Novos Materiais Microporosos

# Developing Novel Microporous Materials

Dissertação apresentada à Universidade de Aveiro para cumprimento dos requisitos necessários à obtenção do grau de Mestre em Química Inorgânica e Materiais, realizada sob a orientação científica do Doutor Zhi Lin, Investigador do Centro de Investigação em Materiais Cerâmicos e Compósitos (CICECO) no Departamento de Química da Universidade de Aveiro.
A dissertation presented to the University of Aveiro in partial fulfillment of the requirements for the awarding of the master degree in Inorganic Chemistry and Materials carried out under supervision of Doctor Zhi Lin, Researcher at Research Center for Ceramic and Composite Materials (CICECO) at Chemistry Department of the University of Aveiro.

Apoio financeiro da FCT e do FSE no âmbito do III Quadro Comunitário de Apoio.
Ref.ª PTDC/CTM/73643/2006

“Nothing in life is to be feared, it is only to be understood. Now is the time to understand more, so that we may fear less.”
Marie Curie

**o júri**

president

Prof. Doutor Artur Manuel Soares da Silva
professor catedrático do Departamento de Química da Universidade de Aveiro

Doutor Stanislav Lazarov Ferdov
investigador Auxiliar do Departamento de Física da Universidade do Minho

Doutor Zhi Lin
investigador do CICECO no Departamento de Química, Universidade de Aveiro

**agradecimentos**

I would like to express my sincere gratitude to all those who contributed for the possibility of completing this thesis.

I am sincerely and truly grateful to my supervisor, Dr. Zhi Lin, who was always supportive and comprehensive, and willing to listen and discuss the work as well as for all the given advice.

I would also like to thank Dr. Rosário Soares for all the XRD analysis, Eng[a] Marta Ferro for all the help in SEM characterization and Celeste Azevedo for the assistance in the laboratory and in the utilization of equipments. To all the members of the Chemistry Department and of the laboratory, I am grateful for all the transmitted knowledge and for the friendly environment, namely Dr. Paula Brandão, Dr. Duarte Ananias, Dr. Fanian Shi, Dr. Zhengying Wu, Dr. Xiaowei Li, Andreia Machado and Mengistie Leweyehu.

I would also like to thank all my family for endless support, interest and motivation. To my mother, aunt, sisters, nephews and to the rest of the family a sincere Thank You!

To my colleagues and long standing friends Joana, João and Frederico, thanks for being there, still, after so many years. We are again co-workers and colleagues but have never stopped being friends!

For all the companionship, laughter and advice, thanks to the friends and colleagues of the Chemistry Department of University of Aveiro.

Last, but not least, to all my friends, older ones, recent ones, from Covilhã, Coimbra (thank you), Aveiro, Sobral and from all around, even if you do not even imagine it, you helped a lot in the process of finishing this work.

Thank you all!

**palavras-chave**

materiais microporosos, estruturas cristalinas, síntese hidrotérmica, ETS-4, substituição isomórfica, fosfatos de vanádio, condições de síntese.

**resumo**

Os materiais microporosos têm elevado interesse científico e industrial, principalmente devido às suas propriedades, tais como catálise selectiva, separação selectiva e troca iónica, directamente relacionadas com a sua estrutura. De modo a desenvolver novos materiais, com novas propriedades, ou para ajustar propriedades de materiais já conhecidos, estudos sistemáticos nesta área são usuais, especialmente em relação aos processos de síntese de materiais microporosos.

O principal objectivo deste trabalho é o de sintetizar e caracterizar novos materiais microporosos, partindo do ajuste da síntese do material ETS-4 e de um estudo sistemático de uma composição de fosfato de vanádio.

O ETS-4 é um óxido misto sintético conhecido, que contém átomos de Ti em coordenação octaédrica e piramidal quadrada, em conjunto com unidades silicato tetraédricas. A sua estrutura distinta possui cadeias de titânio que se podem comportar como fios quânticos. O ETS-4 também exibe o efeito "portão molecular", o que significa que a abertura do poro pode ser ajustada consoante a temperatura, melhorando as características de separação do material. Neste trabalho, tentou-se substituir isomorficamente o Fe pelo Ti no ETS-4, sendo a substituição bem sucedida através de síntese hidrotérmica directa. A adição de tricloreto de ferro no precursor não modifica significativamente o processo de cristalização da síntese do ETS-4. Várias técnicas de caracterização, tais como difracção de raios-X de pós, SEM/EDS, infravermelho, Raman $^{29}$Si MAS NMR, foram utilizadas para estudar a incorporação do Fe no ETS-4. Comparando amostras directamente sintetizadas com amostras resultantes de troca iónica, conclui-se que o Fe não se encontra nos poros das amostras directamente sintetizadas. A estabilidade térmica destas amostras é semelhante à do ETS-4, enquanto que a de amostras resultantes de troca iónica é muito menor.

A família dos fosfatos de vanádio apresenta uma grande variedade de estruturas cristalinas visto o vanádio existir em vários estados de oxidação (III, IV, V) e em diferentes geometrias de coordenação (tetraédrica, piramidal quadrada e octaédrica regular e distorcida). O principal interesse científico nos fosfatos de vanádio surge das suas aplicações como catalisadores e também das suas interessantes propriedades electroquímicas e magnéticas.

O estudo desta família de materiais foi feito segundo o sistema $VOSO_4$ – $NaH_2PO_4$ - $H_2O$ – aditivos. A influência das condições da síntese e dos aditivos foi estudada sistematicamente. Vários parâmetros tais como temperatura, solvente, fonte de aquecimento e a presença de aditivos orgânicos foram testados. Este tipo de estudo, sob diferentes condições, pode resultar em produtos finais cristalinos com estruturas conhecidas (obtidos por diferentes reacções) ou em fases cristalinas que precisam de ser posteriormente descritas. $NaVOPO_4$, $Na_3VO(PO_4)(HPO_4)$ e um material com estrutura semelhante a $Na_3VO_2(PO_4)F$ foram obtidos através de precursores sem aditivos orgânicos, com misturas eutéticas (cloreto de colina e ureia) e com ácido maleico (2 semanas de síntese), respectivamente. A adição de ácido maleico (entre 10 h e 7 d de síntese) e de ureia resultou em dois produtos cristalinos que não foram identificados na base de dados de raios-X como sendo puros ou uma mistura de fases cristalinas.

**keywords**

microporous materials, crystalline structures, hydrothermal synthesis, ETS-4, vanadium phosphates, isomorphous substitution, synthesis conditions.

**abstract**

Microporous materials have high scientific and industrial interest, mainly due to their structural related properties like selective catalysis, selective separation and ion-exchange. In order to find new materials with new properties or to fine tune properties of known materials, systematic research in this area is usual, especially concerning synthesis procedures of microporous materials.

The main goal of this work is to synthesize and characterize new microporous materials, starting from tuning the syntheses of ETS-4 material and a systematic synthesis research of a vanadium phosphate composition.

ETS-4 is a well known synthetic mixed oxide that contains Ti atoms in octahedral and square-pyramidal coordination, along with tetrahedral silicate units. Its distinct structure possesses titania chains that can behave as quantum wires. ETS-4 also displays “molecular gate effect”, which means that the pore opening can be tuned with temperature, giving the material enhanced sieving characteristics. In this work, Ti isomorphous substitution by Fe was attempted and proved successfully through direct hydrothermal synthesis. The addition of iron trichloride in precursor does not significantly modify the crystallization process of ETS-4 synthesis. Several different characterization techniques, such as powder XRD, SEM/EDS, Infrared, Raman, $^{29}$Si MAS MNR, were used to study the incorporation of Fe in ETS-4. By comparison of direct synthesized and ion exchanged samples, it is concluded that Fe is not in pore of the direct synthesized samples. The thermal stability of the direct synthesized samples is similar to the parent ETS-4 while the ion exchanged one shows much low stability.

Vanadium phosphate family can present a great variety of crystalline structures, since vanadium can exist in various oxidation states (III,IV,V) and different coordination geometries (tetrahedral, square-pyramidal, distorted and regular octahedral). The major scientific interest in vanadium phosphates arises from their applications as catalysts, but they also present interesting electrochemical and magnetic properties.

Synthesis research has been carried out in $VOSO_4$-$NaH_2PO_4$-$H_2O$-additives system. The influences of synthesis conditions and additives on the final product were studied systematically. Several parameters, such as temperature, solvent, heating source and presence of organic additives, were tested. These syntheses under different conditions can result in crystals with known structures (obtained through different synthesis routes) or in new crystalline phases that need to be further characterized. $NaVOPO_4$, $Na_3VO(PO_4)(HPO_4)$ and a material with the structure similar to $Na_3V_2O_2(PO_4)_2F$ have been obtained from precursors without any organic additives, with eutectic mixtures (choline chloride and urea), and with maleic acid (2 weeks’ synthesis), respectively. The addition of maleic acid (between 10h and 7 d of synthesis) and urea resulted in two crystalline products which cannot be identified as existed single or mixed phase from XRD database.

## Table of Contents

**List of Abbreviations**

| | |
|---|---|
| AlPO | aluminophosphate |
| 2D DHAF | two-dimensional quantum Heisenberg antiferromagnet |
| AM-1 | Aveiro-Manchester material 1 |
| AM-2 | Aveiro-Manchester material 2 |
| AM-3 | Aveiro-Manchester material 3 |
| AM-4 | Aveiro-Manchester material 4 |
| ChCl | choline chloride |
| CT | charge transfer |
| DR UV-Vis | diffuse reflectance ultraviolet-visible |
| DSC | differential scanning calorimetry |
| EDS | energy dispersive spectroscopy |
| ETS-10 | Engelhard TitanoSIlicate 10 |
| ETS-4 | Engelhard TitanoSilicate 4 |
| FTIR | Fourier transformed infrared |
| GTS-1 | Grace Titanium Silicate-1 |
| IR | infrared |
| LTA | Linde Type A |
| M | metal ion |
| MAS NMR | magic angle spinning nuclear magnetic resonance |
| MeAlPO | metal aluminophosphate |
| MFI | Mutinaite |

| | |
|---|---|
| MOR | Modernite |
| MPMD | 2-methyl pentamethylenediamine |
| MR | membered ring |
| O | octahedral |
| OPT | octahedral-pentahdral-tetrahedral |
| SAPO | silicon-aluminophosphate |
| SBU | secondary building unit |
| SEM | scanning electron microscopy |
| T | tetrahedral |
| TMS | tetramethylsilane |
| UND-1 | University Notre Dame material 1 |
| VPO | vanadium phosphate |
| XRD | X-ray diffraction |

**List of Figures**

**List of Tables**

# CHAPTER 1
# INTRODUCTION

# 1. INTRODUCTION

## 1.1 Microporous materials

Microporous materials, commonly known as Open-Framework structure materials, consist of a class of inorganic materials that possess regular pores or voids. A frequently used term in materials science is “molecular sieve” that refers to porous materials that can distinguish molecules on the basis of size and shape [1]. One of the most well known families of this type of materials is the zeolite.

The development of crystalline microporous materials started in the late 1940’s from the preparation of synthetic zeolites, that consist of interconnected $[SiO_4]^{4-}$ and $[AlO_4]^{5-}$ [2] [3]. In the following 30 years, zeolites with various topologies and chemical compositions were prepared. A breakthrough leading to an extension from zeolites to non-aluminosilicates occurred in 1982 when Flanigen *et al*. [4] reported the synthesis of aluminophosphate molecular sieves (AlPOs), that was then followed by the development of substituted aluminophosphates [1], silicon-aluminophosphates (SAPOs), metal aluminophosphates (MeAlPOs) etc, as it can be seen in Figure 1.1. Since then, crystalline microporous materials have been synthesized in a wide range of compositions and by several different methods, to fulfil a large and growing number of purposes and applications.

Crystalline microporous materials usually consist of rigid three-dimensional frameworks with hydrated inorganic/organic cations or organic molecules located in the cages/cavities (pores) or channels of the inorganic or hybrid organic-inorganic host framework. These materials generally have a narrow pore size distribution that makes them able to be selective in molecular level base.

Porous materials are often classified according to their pore size: pore sizes bellow 2 nm are called microporous, those in the range of 2-50 nm are denoted as mesoporous and those above 50 nm are macroporous [1].

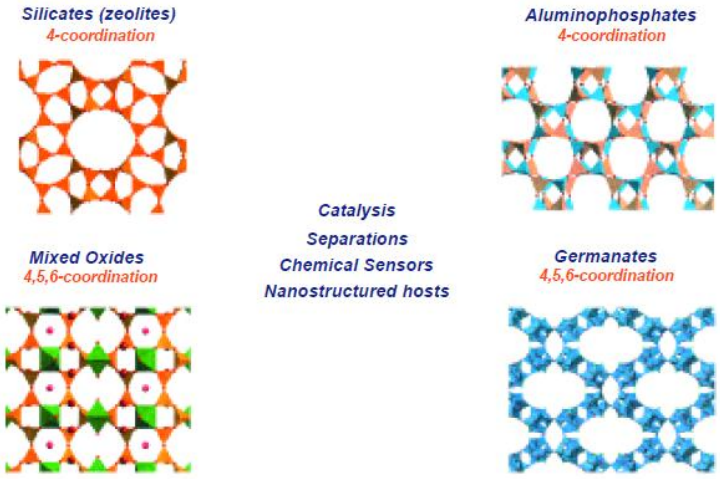


**Figure 1.1-** Some examples of 'molecular sieve' materials and some of their applications. Different types of structures and different types of coordination of the atoms that build the tridimensional framework are represented [5].

### 1.1.1 Zeolites

Over 200 years ago, Swedish scientist Crønstedt discovered stilbite [6], the first crystalline microporous aluminosilicate. Upon heating, the mineral released water, and that gave these materials their general name, zeolite, after the Greek *zeo* (to boil) and *lithos* (stone) [7]. Due to its unique structure, zeolites possess remarkable features, the most important being selective sorption (molecular sieving), ion exchange and catalytic activity, and many of these features benefit from the high ordered structure that these types of solids possess [4].

Zeolites have been considered as crystalline three-dimensional aluminosilicates with open frameworks. Their structures are built up of $[SiO_4]^{4-}$ and $[AlO_4]^{5-}$ tetrahedra linked to each other by sharing all oxygen atoms, to form regular intercrystalline cavities (pores) and channels of molecular dimensions [9], as depicted in Figure 1.2. Silicon-oxygen tetrahedra create neutral framework when connected in a three-dimensional network. The replacement of $Si^{IV}$ by $Al^{III}$ in this type of structures creates a charge imbalance, and to preserve the neutral charge of the overall structure, each $AlO_4$ tetrahedron needs a balancing charge

that is provided by exchangeable cations which are held electrostatically in the void of zeolite structure [9].

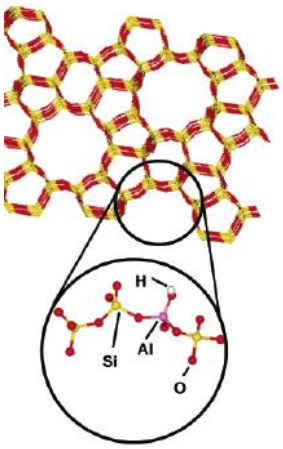


**Figure 1.2-** Example of a zeolite structure, ZSM-5. It can be seen in detail the Si an Al atoms in tetrahedral coordination, linked by shared oxygen atoms [10].

The stability of zeolites varies greatly depending on framework topologies and chemical compositions such as the Si/Al ratio, and the type of charge balancing cations. Natural zeolites are chemically represented by the empirical formula

$$M_{2/n}O : Al_2O_3 : y\ SiO_2 : wH_2O$$

where M is the cation, y is equal or greater than 2, n is the valence of cation and w is the water contained in the voids of the zeolite [1].

Zeolites and zeolite-type oxides (zeotypes) are classified according to their framework types. A framework type is determined based on the connectivity of the tetrahedral atoms and is independent of chemical compositions, types of extra-framework species, crystal symmetry, unit cell dimensions or any other chemical and physical properties [1]. Figure 1.3 gives some examples of zeolites.

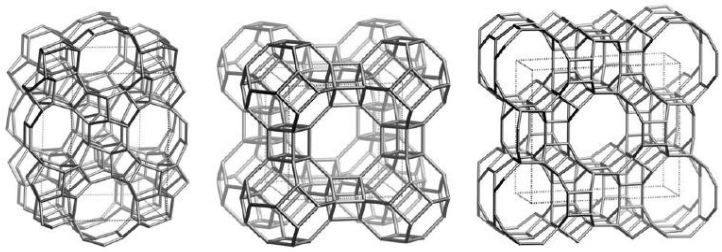

**Figure 1.3-** Examples of zeolitic structures, with different topologies (MFI, LTA and MOR topologies respectively) [11].

One of the most important structural features of zeolites is the size of the pore opening because that will determine its possible applications and performance. The pore size is generally related to the size of the ring that is defined by the number of tetrahedral atoms forming the pore. According to the literature [12], zeolites can also be defined as small-pore (8-ring), medium-pore (10-ring) and large-pore zeolites (12-ring).

All zeolite structures are built up from $TO_4$ tetrahedra, which are called primary (or basic) building units. Although the individual $TO_4$ tetrahedron, the primary building unit, can describe zeolite structures, the secondary building units (SBU) (Figure 1.4), based on small groups of linked tetrahedra, are needed to describe and systematize their topologies. These structural building units can be defined as finite structures that can alone, or in combination with another one, build up the whole framework [1].

Currently, many different zeolite structures are known, and a variety of metals has been successfully incorporated into zeolite frameworks, such as Ti, B, Ga, Fe, Cr, V, Mn, Zr, Zn, etc. [13].

Microporosity makes zeolites powerful tools in selective catalysis and adsorption, and some examples of those applications are described in Figure 1.4. But this type of materials also presents some disadvantages. Zeolite systems present some limitations because its framework constituents are normally boron, aluminum, gallium, silicon and phosphorous bridged by oxygen atoms, making

these materials oxides of the III to V groups and of second and third period, which makes their frameworks insulators. This can be a problem for catalysis and for possible optical applications [14].

This has acted as a motivation for many scientists and for the progress of their work as the quest for new compounds, with porous frameworks and that exhibit new properties, and are possibly used in a very wide range of areas. This effort has broadened the definition of zeolites and zeotypes, and now, many types of microporous materials have been studied. Concerning microporous materials, many of the synthetic procedures, types of structures, characterization methods, and properties are no longer restricted to the zeolite family or the aluminophosphate family.

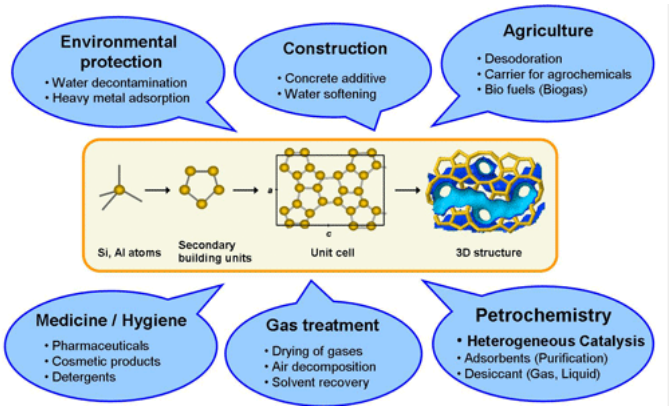


**Figure 1.4-** Examples of the "construction" of zeolites and microporous materials, and some applications [15].

## 1.2 Synthesis

The synthesis of microporous materials is a field in progress. The final crystalline phase can be obtained through many different routes and can depend on several different factors. Its complete study can include the chemical,

thermodynamic and kinetic characterization of all the process involved in the formation of a specific phase.

In microporous material chemistry, hydrothermal reactions are commonly used. But, since the chemistry of microporous materials is now very diverse, the synthesis methods can differ in the solvents or in the energy source used for synthesis, for example.

### 1.2.1 Hydrothermal synthesis

Zeolites and zeotypes are usually synthesized in hydrothermal conditions, in order to obtain a crystalline final product, normally a powder. The term 'hydrothermal' came from the geosciences, where it implied a regime of high temperatures and water pressures [12]. In the hydrothermal process, reagents are usually dissolved or dispersed in water, and then heat-treated at elevated temperatures, in an apparatus called autoclave, as the one depicted in Figure 1.5. For reactions at moderate temperatures (up to 250 ºC), the autoclaves are normally lined with Teflon. If higher reaction temperatures are desired, the reactions can be carried out in stainless steel or gold tubes [14]. In hydrothermal experiments, there are some requirements for the starting materials (reagents), like having an accurately known composition and they must be as homogeneous, fine and pure as possible [14].

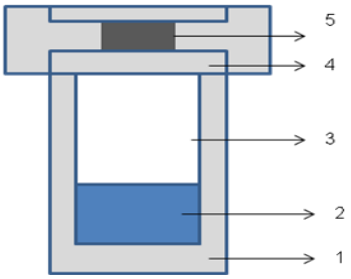


**Figure 1.5-** Schematic example of a stainless steel autoclave, 1- stainless steel autoclave, 2- precursor mixture, 3- teflon liner, 4- stainless steel lid, 5- spring.

Normally, the final products are not the thermodynamically most stable product, but rather a material that is the result of a kinetically controlled synthetic pathway [8]. Although crystallization of microporous materials is an important subject, as well as the thermodynamics and kinetics of nucleation and crystal growth events, we shall not discuss them in the detail in this work.

Many parameters can influence this process, and they can also be used to control the final product of the synthesis, such as:

**composition:** the reagents, that are used as the source of components to form the final framework, are of extreme importance. Their purity level and relative ratios can determine the final structure. For a complete knowledge of a crystalline structure, one needs know the precise molecular composition of the final product.

**pH:** usually hydrothermal synthesis of zeolites happens at high pH, and it is normal that during the crystallization process it becomes even higher. The pH of the solution is important because it can indicate the amount of OH ions in solution, and also influence the formation of specific crystalline phases.

**time:** each crystallization process has an optimal period of time to occur, that is called the ‘induction period’, being the time that passes since reaction begins until crystallization starts [16]. This parameter depends on the system in study, composition, temperature etc. Hydrothermal synthesis can be carried out from just a few hours up to several months to execute crystallization process.

**temperature:** temperature is an important factor which influences the obtained phase and can alter the ‘induction period’. At higher temperature, the crystallization rate is also higher.

**mechanical factors:** whether stirring of the synthesis mixture (for example) can influence in a great extent the formation of a certain crystalline phase, because it can influence the processes involved during the crystallization, such as formation and assembling of the nuclei, etc.

**templates and structure directing agents (SDA):** templates are chemical species (cations or neutral species) that play a role in stabilizing the structural subunits that are thought to be the constitution of the final crystalline product. A species is considered to be a template or SDA if, upon its addition to the reaction mixture, crystallization is induced to generate a specific microporous structure that could not be formed in absence of the agent [16]. Normally, they are organic species, like organic amines and quaternary ammonium ions. It is believed that these additives can play some different roles in the synthesis of microporous materials, such as;

a) behave as Templates or SDAs

b) act as gel modifiers, which result in the formation of structures that would not be formed in absence of the organic additive

c) interact chemically with other components of the gel, altering its character

d) interact physically with other components of the gel, altering the characteristic of the gel, solubility of the species, aging characteristics, transport and thermal properties and time of crystallization

e) act as a void filler [16].

All factors influence the crystallization process. New routes and techniques of synthesis may lead to the finding of new structures or compositions of microporous materials, and they should be explored.

### 1.2.2 Microwave synthesis

Although the synthesis of molecular sieves is normally conducted in water or other solvents in a sealed container (like an autoclave), under hydrothermal or solvothermal conditions in conventional oven [17], recently, several different synthesis methods have been developed, for example, microwave dielectric heating synthesis.

Microwaves are a form of electromagnetic energy and are located in the 1 mm to 1 nm range of the electromagnetic spectrum (corresponding to frequencies between 100 and 5000 MHz) [18]. Microwave dielectric heating is widely used in organic synthesis, analytical chemistry and inorganic synthesis, and has been used in the hydrothermal synthesis of molecular sieves. This has allowed faster crystallization rates and higher selectivity when compared to conventional heating [17].

In conventional heating processes of a mixture, the heating is from the surface to the interior of the reaction vessel, so the energy is transferred from the surface to the bulk of the mixture and subsequently, to the reactive species [18]. In microwave assisted synthesis, microwaves heat the bulk of the mixture by dielectric loss from the irradiated sample [17], or in other words, by the absorption of the amount of electromagnetic energy that the mixture is exposed to [18]. One of the requirements is that the components in the reaction mixture need to be able to absorb microwave radiation.

These characteristics make microwave assisted heating a more effective, faster and homogeneous synthesis method. The synthesis time can be reduced from days to hours, for example. Because the energy and time that are required in microwave synthesis are significantly lower, this heating process is also more energetically efficient and environmentally friendly.

Like in hydrothermal synthesis, microwave assisted synthesis also has several requirements and specific parameters that need to be carefully controlled, like temperature, pressure, pH of the synthesis mixture, etc., and also, because this technique is performed in more sophisticated apparatus, more attention to the all process is needed. The vessel where the reaction is carried out has some differences when compared with autoclaves used in hydrothermal synthesis (Figure 1.6).

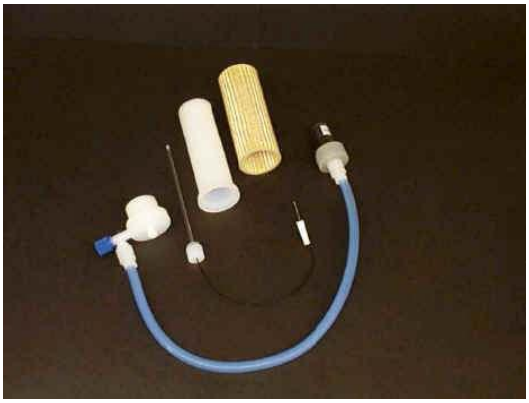

**Figure 1.6-** Reaction vessel of a microwave heating apparatus, CEM Mars 5 Microwave Accelerated Reaction System. From left to right there are the vessel lid with the pressure release valve, the temperature sensor (sapphire or glass tube with optic fiber temperature sensor inside), the Teflon reaction vessel, the Kevlar explosion proof sleeve and the pressure transducer (attached to the pressure valve) [19].

The main synthesis parameters that should be taken into account are the pressure that cannot be too high because of the risk of explosion, the temperature and also the pH of the mixture, because that can damage the temperature sensor.

A large number of materials have already been synthesized through the microwave assisted heating process, for example aluminophosphates, nano materials, and several types of zeolites.

### 1.2.3 Ionothermal synthesis

Another alternative to hydrothermal synthesis is to use non-aqueous solvents instead of water, for example, ion liquids.

Ion liquids belong to a class of organic solvents with high polarity and a pre-organized solvent structure. They can be defined as liquids at ambient temperatures that consist of ions and have excellent solvating properties, low measurable vapor pressure and high thermal stability [20]. One can use a broader

definition in the area of materials synthesis of an ion liquid as any salt that melts below the temperature used in the synthesis of zeolites/zeotypes (150-200 ºC) [21].

When using ion liquids or related solvents in zeolite and microporous material synthesis, one can use the term “ionothermal synthesis”. The main difference between normal hydrothermal/sovothermal synthesis and ionothermal synthesis is that the solvent is ionic in nature, instead of molecular, so, the ion liquid can act as both the solvent and template or cation provider for the synthesis, because the constituents of the ionic liquid can be structurally and chemically similar to template species [20]. Ionic liquids have very low vapor pressures, so the safety problem associated with the high pressures used in hydrothermal synthesis is eliminated, and makes this solvent proper to use in microwave synthesis (for example). Because no other solvents are used (maybe only residual amounts of water), ideally, ionothermal synthesis removes the competition between template-framework and solvent-framework interactions, as depicted in Figure 1.7, leading to pure final phases [20].

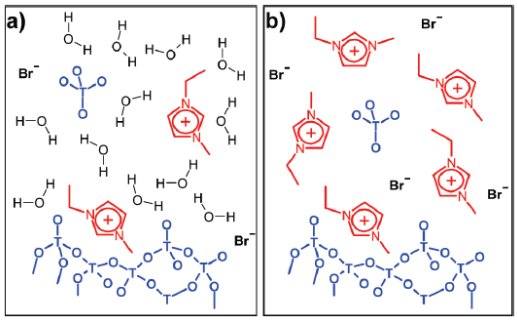


**Figure 1.7-** Comparison between hydrothermal synthesis **(a)** and ionothermal synthesis **(b)**. The dominant interactions are: (a) between water (solvent) and the template or framework, and (b) between the template and framework [20].

In alternative to ionic liquids, eutectic mixtures can also be used as solvents. An eutectic mixture can be defined as a mixture of two or more compounds with a melting point lower than any of its components [20]. The

properties of eutectic mixtures are very similar to the ones of ionic liquids, but they present the advantage of being more easily prepared in the pure state, they are nonreactive towards water, biodegradable and cheaper than ion liquids. Some examples of eutectic mixtures are based on the mixture of choline chloride and urea or malonic acid, in well defined proportions.

## 1.3 Properties

Many applications of microporous materials are related to their unique structure. These materials present high internal surface areas, high thermal stability, ion exchange properties and molecular sieving effect. Their frameworks and properties can even be altered through isomorphous substitution. Some of these properties are described here. Catalysis, and specifically selective catalysis benefits greatly from all of this properties and is one of the main applications (industrially and in a smaller scale) of microporous materials, but that topic will not be discussed in detail in this work.

### 1.3.1 Ion exchange

Microporous materials exhibit ion exchange capacity. Ion exchangers are, by definition, insoluble solid materials which can carry exchangeable cations or anions [22]. These ions can be exchanged for a stoichiometrically equivalent amount of other ions of the same charge when the ion exchanger is in contact with an electrolyte solution [22].

Ion exchangers owe their characteristic properties to a peculiar feature of their structure. In the case of microporous materials, the peculiar feature is the three dimensional structure that possesses pores, channels and voids. In the case of zeolites and most zeotype materials, the framework has an overall negative charge, that needs to be balanced by cations that fill the voids of the three

dimensional framework (extra-framework cations or species). These extra-framework cations can be exchanged by other cations. This exchange depends on several factors like nature of the cation species, cation size, cation charge, temperature, concentration of the cations in solution, solvent, and of course, the ion exchanger (the microporous material) itself, the structural characteristics. Thus, ion exchange may alter the properties of the material being considered, like its stability, catalytic activity, overall topology, etc. In other words, ion exchange allows the fine tuning of microporous materials properties.

### 1.3.2 Molecular sieving

The most important feature that microporous materials present is probably their ability to separate molecules or species based on their size and shape. That ability is called molecular sieving.

This happens mainly due to the regular pore size system present in these materials. Generally, molecules with dimensions smaller than the pore can pass freely through it while bigger molecules are rejected (Figure 1.8). In zeolites, the discrimination of sizes can occur so sharply that the molecules with even sub-Å size can be separated.

The variability in the dimensions of the pores and their very high internal surface area are the main responsible for the catalytic shape/ size selectivity. Sieving effect is intimately related with the material structure and its composition.

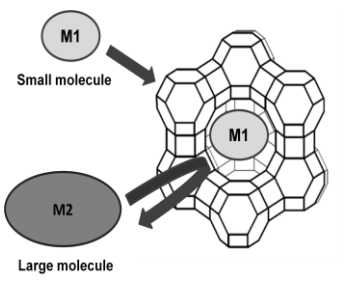


**Figure 1.8-** The molecular sieving effect

### 1.3.3 Isomorphous substitution

By definition, isomorphic substitution is considered to be the replacement of an element in a crystalline lattice by another element with similar cation radius and coordination requirements [23]. This is normally achieved by adding the source of the element to be incorporated in the synthesis mixture.

Isomorphous substitution is important in molecular sieves and microporous materials, because it can result in novel materials, with important redox and catalytic properties, for example in AlPOs [24] and in titanosilicates.

## 1.4 Titanosilicates

Normally, the frameworks of zeolite and microporous oxide materials (AlPOs, SAPOs, MeAlPOs, etc) are constituted by atoms in a tetrahedral coordination. Microporous structures comprised entirely of octahedral sites are also known [25]. Since the early 1990's, mixed octahedral-pentahedral-tetrahedral (OPT) microporous frameworks have been studied [25]. Recently, there has been a lot of research aimed at preparing inorganic microporous framework solids containing atoms with different coordination geometries. One series of those types of materials are the microporous titanosilicates and related materials, which contain $Ti^{4+}$ atoms usually in octahedral coordination [26].

The search for novel multifunctional materials has led to the successful preparation of a number of microporous and layered titanosilicates with potential applications in catalysis, ion exchange and separation processes [27]. In microporous titanosilicates, titanium atoms are usually in octahedral $[TiO_6]^{2-}$ units and silicon atoms in tetrahedral $[SiO_4]$ units, and the manner of their connection predetermines what type of framework is formed. This type of materials is normally formed in $Na_2O$-$K_2O$-$SiO_2$-$TiO_2$-$H_2O$ system, under hydrothermal conditions.

Titanosilicates were first mentioned in a 1967's report [29], where the synthesis of titanium silicates in similar conditions to those of aluminosilicates was mentioned [30]. Later, in 1973, a naturally occurring alkaline titanosilicate identified as zorite was discovered in trace quantities in the Siberian tundra, and the structure of this mineral was then described [31]. The structure of this mineral is characterized by a highly disordered framework with a two-dimensional channel system. Two orthogonal sets of channels are defined by 12-T/O atom and 8-T atom rings (T= tetrahedral silicon; O= octahedral titanium). The disorder in the mineral zorite results in the 12-ring channels being partitioned into sections. A molecule diffusing into this 12-T/O ring channel must make detours through the 8-T ring channel system, so, the adsorption characteristics of zorite are far inferior to those expected for an unfaulted material. Zorite also lacks thermal stability, as water acts as part of the structure, forming chains through the channel system. When water is removed, the framework structure collapses [30].

In 1989 and 1990 two independent reports by Kuznicki and Chapman and Roe [32] [33] presented a synthetic structure that appears to mimic the natural mineral zorite, particularly based on the similarities in the powder XRD data. Kuznicki refers the material as ETS-4 and describes it as not very thermally stable and with poor adsorption characteristics. Along with ETS-4, another material, ETS-10, was described.

ETS-10 displays wide pore characteristics [30]. It is considered to be built up from corner-sharing $SiO_4$ tetrahedra and $TiO_6$ octahedra linked through bridging oxygen atoms. The pore structure of ETS-10 contains 12-rings in all three dimensions [25]. ETS-10 is a wide-pore and thermally stable material that presents excellent diffusion and molecular sieving characteristics [25].

A few studies have been done in the field of membrane reactors, specifically ETS-10 and ETS-4 membranes, because the applications of molecular sieves sometimes require membranes instead of powders [25]. Zeolite membranes and films are commonly used in separations, membrane reactors and sensors, and the use of microporous titanosilicate membranes over traditional ones, may present some advantages [34].

There are other known titanoslicates, most of them are synthetic counterparts of natural minerals, and most of the studies that have been done are to explore their ion exchange properties [25]. To date, there are at least 10 structurally proved synthetic open framework titanosilicates, such as AM-1, AM-2 (the titanosilicate analogue of the zirconium silicate mineral umbite), AM-3 (synthetic penkvilksite-2O), AM-4 (the synthetic analogue of lintisite), ETS-4 (synthetic zorite), ETS-10, GTS-1 (the titanosilicate analogue of pharmacosiderite), UND-1 (the titanosilicate analogue of the zirconium silicate kostylevite), synthetic vinogradovite and synthetic sitinakite [28].

### 1.4.1 ETS-4

ETS stands for Engelhard Titano Silicate (Engelhard is the company where the material was synthesized), and represents a new class of microporous zeotype containing $Si^{4+}$ in tetrahedral and $Ti^{4+}$ in octahedral coordination, sharing common $O^{2-}$ ions. ETS-4 is one of the most important of this kind of materials [35].

ETS-4 is a small-pore microporous titanosilicate molecular sieve with an ideal stoichiometry of $(Na,K)_2TiSi_{2.5}O_{13}.xH_2O$ and an effective pore size of about 3.7 Å. Its framework consists of chains of corner-sharing $[TiO_6]$ octahedra along the *b* direction with neighboring octahedral in a chain being laterally linked by $[SiO_4]$ tetrahedra that construct two orthogonal sets of channels defined by 12-MRs (12 membered rings) along the *c* direction and 8-MRs along the *b* direction. The accessibility to the channel is limited to narrow 8-MRs due to the faulting of the larger pore [35]. As it has been mentioned before, ETS-4 structure is very close to the one of the natural mineral zorite, and is illustrated in Figure 1.9.

In the Na form, ETS-4 is not thermally stable. The structure remains intact up to 200 ºC and some modifications in the structure and partial destruction are observed in the 250- 300 ºC range, when the bounded water is lost. The ETS-4 structure is contracted when dehydrated and the pore opening is reduced as the dehydration temperature increases this is called ‘molecular gate effect’ [35], and

allows the fine tuning of the sieving characteristics of this material, as it is illustrated in Figure 1.10 and 1.11.

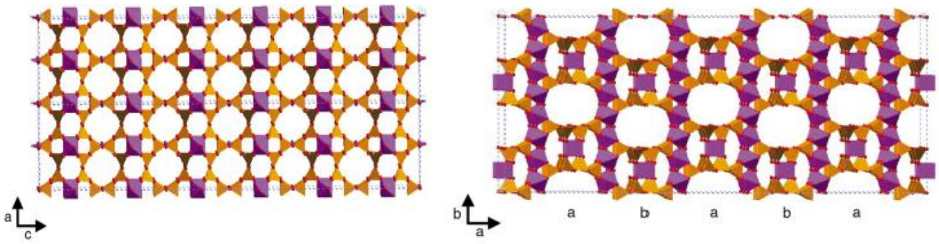


**Figure 1.9-** Two orthogonal projections of ETS-4. In purple are represented the Ti octahedra, in brown the Si tetrahedra and the red spheres are oxygen [9].

Among the titanosilicates, ETS-4 displays good characteristics for size-selective adsorption of molecules and for ion exchange purposes. This material is of high scientific interest since it is the first synthetic mixed oxide microporous molecular sieve material containing octahedral (six-coordinated) and square-pyramidal (five-coordinated) titanium units, in addition to the tetrahedral silicate units [28].

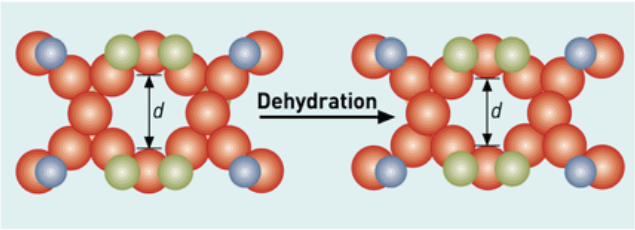


**Figure 1.10-** Illustration of the 'molecular gate effect'. Upon heating, the pore size of ETS-4 is reduced. In red are the oxygen atoms, in green the silicon atoms and in blue the titanium ones [36].

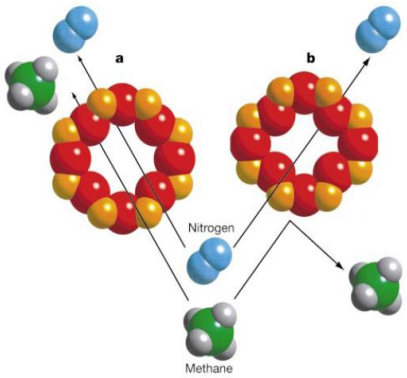


**Figure 1.11-** Example of a titanosilicate (ETS-4), and of its pore size and shape. The difference in the shape of the pore between situation (a) and (b) (the shape of the pore is altered upon heat treatment) makes it selective for nitrogen adsorption only. This can illustrate the molecular sieving effect of titanosilicates [34].

The $TiO_6$ octahedra in the structure of ETS-4 connect each other by corner-sharing, forming –O-Ti-O-Ti-O- chains, and also, the structure contains isolated titanium atoms which are accessible to diffusing/adsorbing species [28]. The –O-Ti-O-Ti-O- chains can exhibit quantum confinement effects and behave as one-dimensional 'quantum wires'. The titanium chains run in the [010] direction (*b* direction) in the framework and the silica matrix provides insulation around the titanium chains [37]. Due to these characteristics, ETS-4 is a potential candidate for applications in optics, electronic devices, optoelectronics, chemosensors and in the field of photochemistry.

In some of its exchanged forms, like $Sr^{2+}$ and $Ba^{2+}$, ETS-4 displays very good properties as a selective adsorbent in gas mixture separations, like natural gas and industrial gases. Also, ETS-4 is a very effective ion exchanger for the removal and storage of radioactive ions and very selective for metals like $Hg^{2+}$, $Pb^{2+}$ and $Cd^{2+}$ [35].

Through incorporation of different atoms in the ETS-4 structure, the range of properties and applications of this microporous titanosilicate can be even wider.

## 1.5 Metal Phosphates

Metal phosphates are a large family of materials that found many applications in diverse areas, being one of the most important as catalysts. Several different metals, including transition metals, have been incorporated into metal phosphate framework. The family studied in more detail during this work, was the vanadium phosphate.

### 1.5.1 Vanadium phosphates

Following the discovery and successful synthesis of the AlPOs family, and the discovery of open-framework materials that have coordination numbers larger than four, much of the work concentrated on the synthesis of phosphates that contain transition metals in their frameworks, because transition metals may exist in framework in different valence states and/or different coordination geometries [38]. Vanadium phosphates (VPOs) are one of such materials.

The interest in this family of materials is mainly due to the catalytic applications of vanadyl pyrophosphate $(VO)_2$-$P_2O_7$ in the selective oxidation of butane to maleic anhydride [38], which is an important step in the functionalization of alkenes that are obtained from petroleum. Also vanadium compounds display interesting redox, electrochemical and magnetic properties.

The various valence states (V, IV, III) and coordination states (tetrahedral, square pyramids, distorted and regular octahedral) of vanadium lead to a large variety in the resulting structures [38]. In VPOs' structures, several situations can occur for the vanadium sub-network, like isolated polyhedra and corner- and edge-sharing chains which are connected to each other by $[PO_4]$ tetrahedra [38].

Since the 90's, many examples of vanadium phosphate materials have been published and characterized, many of them have alkaline or alkaline earth metals or organic molecules in the crystalline structure, and also with templating species. Boudin *et al.* [39] have reviewed and classified several different VPOs and

compared them with each other. The materials are based on the A-V-P-O system (A being a mono or divalent metallic cation), and the structures consist of mixed frameworks built up from different vanadium polyhedra and [$PO_4$] tetrahedra, which delimit tunnels, cages and pores where A cations can move [39]. This review highlights the rich chemistry of the VPOs and the structural variety of the A-V-P-O system, that can be largely attributed to the “flexibility” of the vanadium element.

Vanadium phosphates can possess a large variety of structure types. The examples of some structures given here are divided according to the valence state of the vanadium atoms.

In minerals, vanadium can present three oxidation states, $3^+$, $4^+$ and $5^+$. Trivalent vanadium has the electronic configuration [Ar]$3s^2 3p^6 3d^2$ and occurs mainly in octahedral coordination. Tetravalent vanadium presents the electronic configuration [Ar]$3s^2 3p^6 3d^1$ and can occur in 5- or 6-coordination. Finally, pentavalent vanadium has the electronic configuration [Ar]$3s^2 3p^6 3d^0$ and can present 4-, 5- and 6-coordination.

### 1.5.1.1 Vanadium(III) phosphate structures

The coordination chemistry of vanadium is usually dominated by the +4 and +5 oxidation states. However, in aqueous solutions the +2 and +3 states are also accessible [40], so structures that include V+3 are unusual, but exist. Vanadium(III) complexes characteristically exhibit octahedral geometry, but in the sates from +3 to +5 of the vanadium system, vanadium can adopt square pyramidal and distorted and regular octahedral coordination geometries [40]. One of the first synthesized vanadium(III) phosphates is $Cs[V^{III}_2(PO_4)(HPO_4)_2(H_2O)_2]$, and the structure of this phase is shown in Figure 1.12, where one can see the specific connectivity of the diverse polyhedra and the resulting three-dimensional framework.

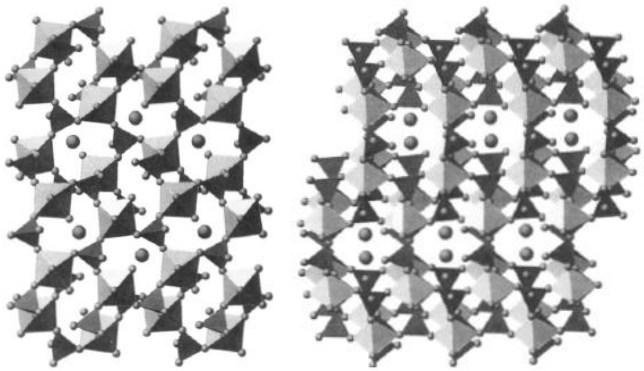

**(a)** **(b)**

**Figure 1.12-** Representation of the structure of $Cs[V^{III}_2(PO_4)(HPO_4)_2(H_2O)_2]$, **(a)** the representation down the *c* axis (with *b* vertical and *a* horizontal), **(b)** down the *a* axis (with *b* vertical and *c* horizontal). The vanadium octahedra and phosphorous tetrahedra, as well as the $Cs^+$ cations are represented [40].

In a work carried out by Vaughey *et al.* [41], the synthesis and characterization of two vanadium(III) phosphates were described. The obtained materials were $VOPO_4.H_2O$ (monoclinic), that is constructed of corner-sharing $[VO_6]$ octahedra, and a second phase $V_{1.23}(PO_4)(OH)_{0.69}(H_2O)_{0.31}.0.33\ H_2O$ (tetragonal) that is built up of face-sharing octahedra, as can be seen in Figure 1.13. These two compounds have similar compositions, but they present very different structures; the only apparent difference in the synthetic conditions is the concentration of the vanadium source. When the vanadium concentration is higher, it favors the formation of the tetragonal phase. This is a good illustration of the structural diversity of the vanadium phosphates, particularly, the vanadium(III) phosphates.

An example of vanadium(III) phosphates in A-V-P-O system is $Ba_3V_2(HPO_4)_6$, that is built up from barium cations and vertex-sharing network of $VO_6$ octahedra and $HPO_4$ tetrahedra units, linked together *via* V-O-P bonds (Figure 1.14) [42].

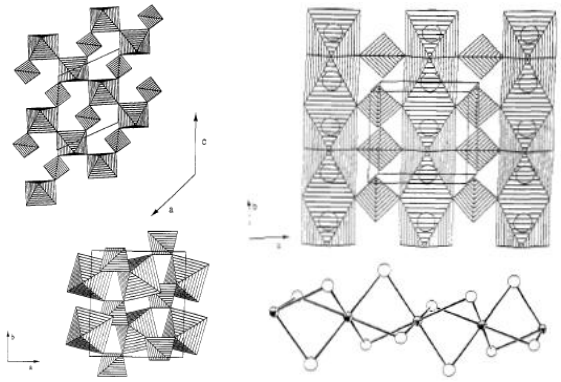

**(a)** **(b)**

**Figure 1.13- (a)** represents the structure of $VOPO_4.H_2O$ and shows the corner-sharing octahedral chains and their connectivity *via* the phosphate groups (views along the *b* direction and along the *c* direction) **(b)** represents the structure of $V_{1.23}(PO_4)(OH)_{0.69}(H_2O)_{0.31}.0.33\ H_2O$ and shows the face-sharing octahedral chains and the tetrahedral phosphate groups. In the bottom is an isolated segment of a face-shared chain [41].

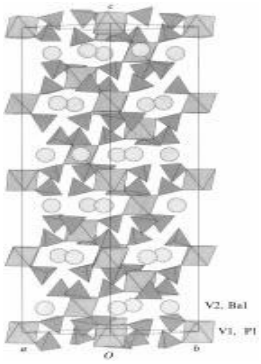

**Figure 1.14-** View of the $Ba_3V_2(HPO_4)_6$ structure down the [110] direction. Octahedra: $VO_6$, tetrahedral: $PO_4$ and spheres: Ba [42].

Another interesting vanadium(III) phosphate is $SnVPO_5$, which has a three-dimensional framework constructed by $V_2O_{10}$ units linked together by tetrahedral phosphate groups and tin atoms located in the structure interstices [43], as depicted in Figure 1.15. This structure is an example of mixed phosphates of Sn(II) and V(III), and it presents magnetic properties.

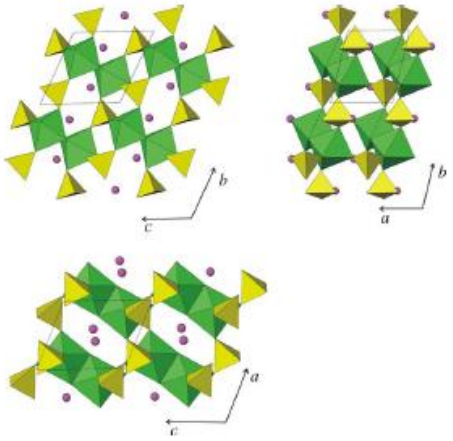


**Figure 1.15-** Projections of the $SnVPO_5$ structure, showing the connection between vanadium (dark green) and phosphate (light green) polyhedra and the location of tin atoms (purple) [43].

An example of vanadium(III) phosphates that presents interesting structure and also ferromagnetic interactions is the $(NH_4)[V(PO_4)F]$ [44]. In this structure (illustrated in Figure 1.16), the trivalent vanadium forms the $VO_4F_2$ octahedra that are linked each other through fluorine atoms and $PO_4$ tetrahedra, resulting in zig-zag chains. This phase presents weak ferromagnetic couplings (interactions).

It is known that, in addition to the applications of vanadium phosphates in heterogeneous catalysis, reduced vanadium systems with low-dimensional structures can also exhibit unusual magnetic behavior, and that may be good for applications in magnetic and electrochemical field [45]. A new example of this family of materials is a recently synthesized sodium vanadium(III) phosphate with a chain structure [45]. The work by Ferdov *et al*. is focused on the mild hydrothermal synthesis, and structure and magnetic characterization of $Na_3V(OH)(HPO_4)(PO_4)$, which is the second inorganic metal phosphate synthesized by the use of 2-methylpentamethylenediamine (MPMD) [45]. However, the formation of this phase is very sensitive to the synthesis condition. Further synthesis research is required to efficiently prepare this material and to explore its unique characteristics (mainly magnetic properties). The structure of this material (Figure 1.17) is built up from one dimensional chains that are composed of corner-sharing $VO_5(OH)$ octahedra running along the *b* direction. These chains are separated by isolated $PO_4$ and

$HPO_4$ tetrahedral units, sharing two of their corners with the neighboring vanadium octahedra. The interconnection between the chains is assured by three distinct $Na^+$ cations [45].

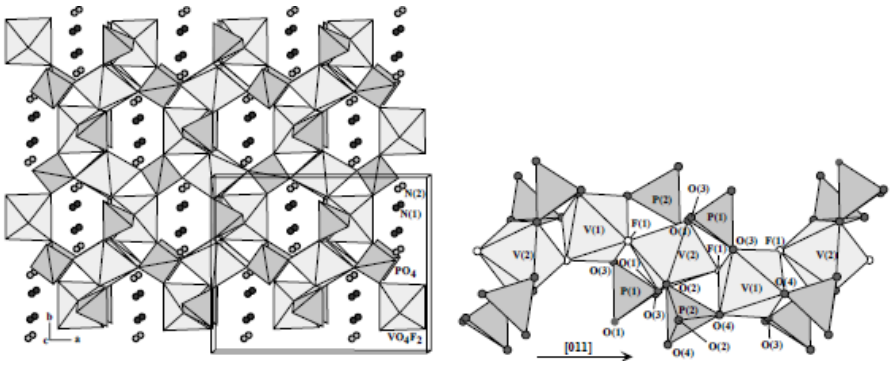


**Figure 1.16-** Polyhedral view of the $(NH_4)[V(PO_4)F]$ structure, showing the three-dimensional framework and the zig-zag chain [44].

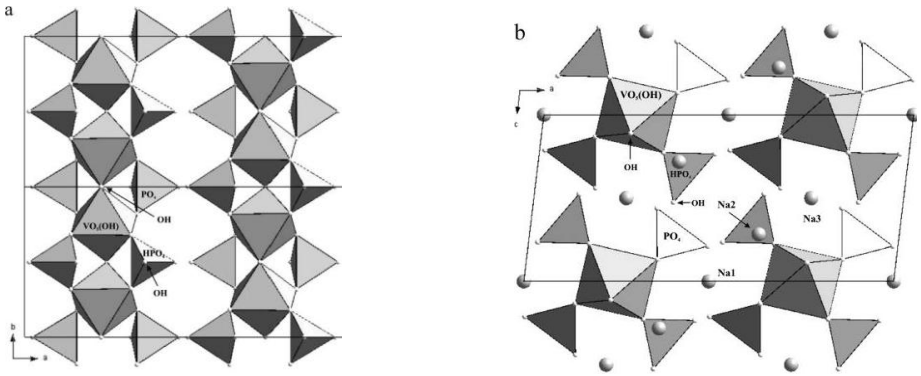


**Figure 1.17-** Structure of $Na_3V(OH)(HPO_4)(PO_4)$ **(a)** along the c direction, **(b)** along the b direction, with the sodium cations properly labeled [45].

Besides being the first sodium vanadium(III) phosphate containing isolated chains of vanadium polyhedra, this phase also shows antiferromagnetic arrangement of the vanadium ions through those chains [45].

### 1.5.1.2 Vanadium(IV) phosphate structures

Many vanadium(IV) phosphates existed, an example given here was reported by Sen *et al.* [46]. They successfully synthesized, through a routine hydrothermal process, a layered vanadium (IV) phosphate material (Figure 1.18), $\{VO(H_2PO_4)_2\}_n$, that demonstrates interesting catalytic and magnetic properties [agree with two-dimensional quantum Heisenberg antiferromagnet [(2D DHAF) model)]. The successful preparation of vanadium (IV) phosphate with this type of magnetic properties may open the doors to the design and synthesis of new vanadium based materials that exhibit DHAF properties.

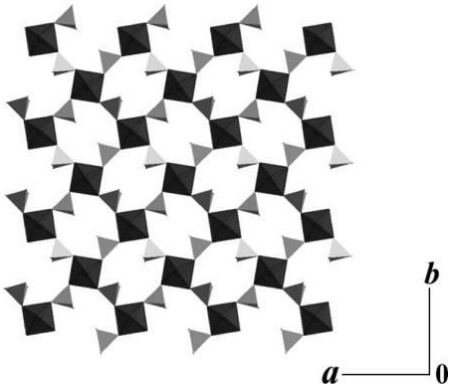


**Figure 1.18-** Example of a layer of the $\{VO(H_2PO_4)_2\}_n$ phase. It shows the interlinking of the $VO_5$ square pyramid and the $H_2PO_4$ tetrahedra forming a (110) layer [46].

### 1.5.1.3 Mixed-valence vanadium phosphates

Another approach in VPO synthesis is to synthesize materials with mixed-valence states, which may lead to the formation of new and interesting structures with new properties, for example larger open of the pores in the framework.

Calin *et al*. reported the synthesis of an open-framework structure with a mixed-valence, $V^{III}V^{IV}(HPO_4)_4.enH.H_2O$, and the product from its calcination at 400 $^oC$, $V^{IV}(HPO_4)_2$ [47]. This structure is depicted in Figure 1.19.

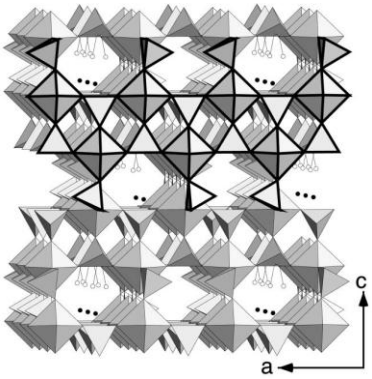


**Figure 1.19-** View along the *b* axis of the structure of the $V^{III}V^{IV}(HPO_4)_4.enH.H_2O$ phase, where tetrahedra and octahedra represent P and V. The ethylenediamine and water molecules are also shown (filled circles) [47].

Normally, in transition metal phosphates, the strict alternation of the transition metal polyhedra and P tetrahedra defines an even ring of polyahedral atoms, like 8, 10, 12, 14, 18 and 20 membered rings and prevents the occurrence of five-ring units (that are very common in aluminosilicate zeolites) [48]. Recently, Cui *et al*. [48] reported the synthesis of $[(C_6H_{16}N_2)_3(VO)(V_2O_4)_2(PO_4)_4.2H_2O]$, templated by trans-1,4-diaminocyclohexane (1,4-DACH). This is a mixed-valence VPO with 7-membered rings, and is described in Figure 1.20.

Because this is a mixed-valence material with novel 7-membered rings (due to the specific connections and structure) it may present novel properties, for example exhibiting the behavior of a ferromagnetic chain compound [48].

Liu *et al.* [49] reported the synthesis of a vanadium phosphate cluster. Specifically, they obtained a closed sphere-like structure of vanadium phosphate compound, $[PV_{2.5}O_{8.8}].3.83\{H_2O\}$, with mixed-valence of vanadium, through a hydrothermal reaction [49]. Besides having an interesting and new structure architecture (Figure 1.21), this compound may possibly be active in photo-oxidation reactions and is a potential photocatalyst.

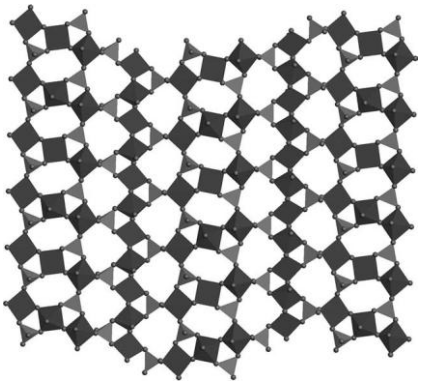

**Figure 1.20-** The inorganic sheet that forms the layer structure of $[(C_6H_{16}N_2)_3(VO)(V_2O_4)_2(PO_4)_4.2H_2O]$, with 3-, 6- and 7-membered rings [48].

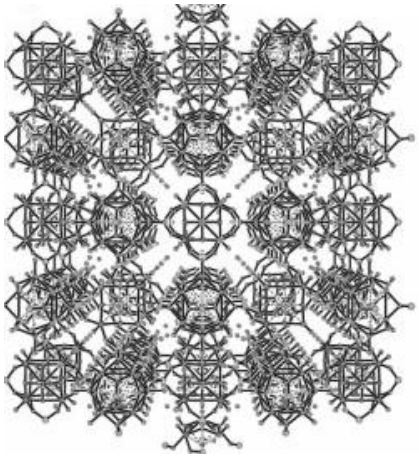

**Figure 1.21-** Packing diagram of the $[PV_{2.5}O_{8.8}].3.83\{H_2O\}$ structure along the *c* axis [49].

## 1.6 Aims of the research

The main purpose of this work is to synthesize and develop novel microporous materials. Through systematic synthesis research, new materials will be synthesized. This is the main driving force in the area of microporous materials chemistry, to develop new materials and find new possible applications for them. ETS-4, a well known microporous material with very good sieving characteristics (mainly in the gas separation field), and a recent sodium vanadium (III) phosphate

structure, with interesting magnetic properties were the main concern of this research.

On a first approach to the synthesis and characterization techniques of inorganic materials, well known ETS-4 will be the subject of the work. Isomorphous substitution and ion exchange experiments will be attempted in order to study its influence on ETS-4 mainly in structural level. XRD, SEM/EDS, DR UV-Vis, Raman, DSC, FTIR and $^{29}$Si MAS NMR are the techniques used to fully characterize as-synthesized materials, providing different structural details and useful training in characterization techniques.

The second part of the work, related to the synthesis of vanadium phosphate, is made in a systematic way. By systematically altering different synthesis parameters (time of the synthesis, used solvents, addition of organic additives), a better knowledge of how the specific synthesis system works and new or different phases can be achieved, which is the ultimate goal of this work.

## 1.7 References

[1] X. Bu, P. Feng, *Crystalline Microporous and Open Framework Materials, The Chemistry of Nanostructural Materials*, Ed. Yang, P., World Scientific (2005) 1.

[2] R. M. Barrer, *J. Chem. Soc.* (1948) 127.

[3] R. M. Milton, *ACS Symposium Series, Zeolite Synth.* 398 (1989) 1.

[4] S.T. Wilson, B.M. Lok, C.A. Messina, T.R. Cannan, E.M. Flanigen, *J. Am. Chem. Soc.* 104 (1982) 1146.

[5] M. Tsapsis, *AlChE Journal* 48 (2002) 654.

[6] A.F. Crønstedt, *Akad. Handl. Stockholm* 18 (1756) 120.

[7] J. C. Van Der Wall, H, Van Bekkum, *J. Por. Mater.* 5 (1998) 289.

[8] M.E. Davis, Nature 417 (2002) 813.

[9] J. Rocha, M.W.Anderson, *Eur. J. Inorg. Chem.* (2000) 801.

[10] C.S. Cundy, P.A. Cox, *Chem. Rev.* 103 (2003) 663.

[11] http://www.iza-structure.org

[12] D.P. Serrano, R. Grieken, *J. Mater. Chem.* 11 (2001) 2391.

[13] S. Sōmiya, R. Roy, *Bull. Mater. Sci.* 23 (2000) 453.

[14] S.A. Schunk, F. Schüt, *Molecular Sieves*, vol. 1, Springer-Verlag Berlin Heidelberg (1998).

[15] http://www.elitenetzwerk.bayern.de/reitmeier_zeolites.0.html

[16] A. Dryer*, An Introduction to Zeolite Molecular Sieves*, John Wile&Sons (1988).

[17] Y. Xu, Z. Tian, S. Wang, Y. Hu, L. Wang, B. Wang, Y. Ma, L. Hou, J. You, L. Lin, *Angew. Chem. Int. Ed.* 45 (2006) 3965.

[18] L.B. Hayes, *Microwave Synthesis- Chemistry at the Speed of Light*, CEM Publishing (2002).

[19] http://www.ietltd.com/pdf_datasheets/Mars5DataSheet.pdf

[20] E.R. Parnham, R. E. Morris, *Acc. Chem. Res.* 40 (2007) 1005.

[21] E.R. Cooper, C.D. Andrews, P.S. Wheatley, P.B. Webb, P. Wormald, R.E. Morris, *Nature* 430 (2004) 1012.

[22] F.G. Helfferich, *Ion Exchange*, McGraw-Hill (1962)

[23] J.C. Jansen, *Science* (1994)

[24] B.M. Weckuysen, R.R. Rao, J.A. Martens, R.A. Schoonheydt, *Eur. J. Inorg. Chem.* (1999) 565.

[25] J. Rocha, Z. Lin, *Reviews in Mineralogy and Geochemistry* 57 (2005) 173.

[26] J. Rocha, P. Ferreira, Z. Lin, P. Brandão, A. Ferreira, J.D.P. Jesus, *J. Phys. Chem. B* 102 (1998) 4739.

[27] V. Kostov-Kytin, B. Mihailova, Y. Kalachev, M. Tarassov, *Micropor. Mesopor. Mater.* 86 (2005) 223.

[28] S. Ferdov, Z. Lin, R.A.S. Ferreira, M.R. Correia, *Micropor. Mesopor. Mater.* 110 (2008) 436.

[29] G. Young, US Pat. 3,329,481 (1967)

[30] A. Philippou, M.W. Anderson, *Zeolites* 16 (1996) 98.

[31] P.A. Sandomirski, N.V. Belov, *Sov. Phys. Crystallograph.* 42 (1979) 686.

[32] S.M. Kuznick, US Pat. 4,853,202 (1989).

S.M. Kuznicki, A.K. Thrust, Eur Pat. 0405978A1 (1990).

[33] D.M. Chapman, A.L. Roe, *Zeolites* 10 (1990) 730.

[34] M.E. Davis, *Nature* 417 (2002) 813.

[35] N.A. Turta, M. Veltri, D. Vuono, P. Luca, N. Bilba, A. Nastro, *J. Porous Mater.* 16 (2009) 527.

[36] M. Freemantile, *Chem. Eng. News* 79 (34) (2001) 15.

[37] B. Yilmaz, Q. Miraglia, J. Warywoda, A. Scco Jr., *Micropor. Mesopor. Mater.* 71 (2004) 167.

[38] A.K. Cheetham, G. Férey, T. Loiseau, *Angew. Chem. Int. Ed.* 38 (1999) 3268.

[39] S. Boudin, A, Guedson. A. Leclaire, M.M. Borel, *Int. J. Inorg. Mater.* 2 (2000) 561.

[40] R.C. Haushalter, Z. Wang, M.E. Thompson, J. Zubieta, *Inorg. Chem.* 32 (1993) 3700.

[41] J.T. Vaughey, W.T.A. Harrison, A.J. Jacobson, *Inorg. Chem.* 33 (2000) 2481.

[42] W.T.A. Harrison, J.H. Buttery , *Acta Cryst.* C 56 (2000) 274.

[43] R.V. Spanchenko, A.S. Mitiaev, V.V. Chernaya, E.V. Antipov, H. Sakurai, E. Takayama-Muromachi, *J. Solid State Chem.* 178 (2005) 3014.

[44] E. Alda, B. Bazán, J.L. Mesa, J.L. Pizarro, M.I. Arritortua, T. Rojo, *J. Solid State Chem.* 173 (2003) 101.

[45] S. Ferdov, M.S. Reis, Z. Lin, R.A.S. Ferreira, *Inorg. Chem.* 47 (2008) 10062.

[46] R. Sen, R. Bera, A. Bhattacharjee, P.Gütlich, S. Ghosh, A.K. Mukherjee, S. Koner, *Langmuir* 24 (2008) 5970.

[47] N. Calin, C. Serre, S. C. Sevov, *J. Mater. Chem.* 13 (2003) 531.

[48] Y. Cui, Y. Sun, H. Meng, G. li, C. Chen, L. Liu, X. Yuan, W. Pang, *Inorg. Chem. Com.* 8 (2005) 759.

[49] Y. Liu, X. Zhang, J. Dou, D. Wang, F. Xu, L. Zhou, H. Su, *Chinese J. Chem.* 24(2006) 135.

# CHAPTER 2

# METHODS AND EXPERIMENTAL

# 2. METHODS AND EXPERIMENTAL

## 2.1 Methods

During this experimental work, several different techniques were used to characterize the structure and morphology of the synthesized microporous materials and the crystalline phases under study, such as, powder X-ray diffraction (XRD), scanning electron microscopy (SEM), diffuse reflectance in the UV-visible region (DR-UV/Vis), infrared (IR) and Raman spectroscopies, and differential scanning calorimetry analysis (DSC). Theoretical fundaments of these techniques will not be discussed in detail in this work, and can be easily found elsewhere.

## 2.2 Experimental

### 2.2.1 ETS-4 experiments

The molar compositions of all the synthesized ETS-4 samples are listed in Table 2.1.

In a typical experiment of hydrothermal synthesis of ETS-4, an alkaline solution was made by dissolving 8.29 g of Sodium Metasilicate (95 wt.% $Na_2SiO_3.5H_2O$, Fluka), 0.5 g of NaOH (Prolabo) and 0.75 g of potassium chloride (99 wt.% Panreac), into 6.35 g of distilled water. The titanium source was then added to the alkaline solution, 7.97 g of titanium trichloride (15 wt.% and 10 wt.% HCl, Merk), and then stirred thoroughly for ca. 1 hour. This solution is then transferred to a Teflon-lined autoclave (45 mL) and treated at 230 ºC for 18 hours, under autogeneous pressure without agitation. After fast cooling with flowing water the samples were filtered, washed with distilled water and dried at 60 ºC for one day.

In the case of isomorphous substitution of Ti by Fe, the previously calculated amounts of Fe were added to the titanium solution using iron trichloride

($FeCl_3$, 99 wt.%, Merck). Fe-ETS-4 samples were obtained by using parent mixture with Ti/Fe ratios 95:5, 91:9, 87:13 and 83:17, resulting in samples Fe-ETS-4(5) – Fe-ETS-4(17). The resulting synthesis gels were transferred into 45 mL Teflon lined autoclaves, and carried out at 230 ºC under autogeneous pressure, for 4 days. After cooling down the autoclaves to room temperature, the products were filtered and washed with distilled water, and dried at 60 ºC overnight.

In ion-exchange experiments, a previously as synthesized pure ETS-4 sample was used. A certain amount of the pure ETS-4 powder was dispersed in water. After that, different amounts of $FeCl_3$ were added to each solution and the suspensions were stirred at room temperature for 6 hours. The resulting samples were ETS-4Fe(10), ETS-4Fe(25) and ETS-4Fe(50). After that, solutions were filtered off and washed with distilled water. The resulting powders were dried overnight at 60 ºC.

**Table 2.1-** Molar fractions and synthesis conditions for ETS-4 samples.

| Sample | Composition (molar fraction) | T (ºC) | Time (days) |
|---|---|---|---|
| ETS-4 | 1.0 $TiO_2$- 5.8 $Na_2O$- 0.6 $K_2O$- 5.0 $SiO_2$- 114 $H_2O$ | 230 | (~18 h) |
| Fe-ETS-4(5) | 0.99 $TiO_2$- 5.75 $Na_2O$- 0.65 $K_2O$- 4.91 $SiO_2$- 113.4 $H_2O$- 0.02 $Fe_2O_3$ | 230 | 4 |
| Fe-ETS-4(9) | 0.98 $TiO_2$- 5.8 $Na_2O$- 0.656 $K_2O$- 4.98 $SiO_2$- 114.07 $H_2O$- 0.04 $Fe_2O_3$ | | |
| Fe-ETS-4(13) | 0.97 $TiO_2$- 5.84 $Na_2O$- 0.66 $K_2O$- 5.02 $SiO_2$- 114.6 $H_2O$- 0.074 $Fe_2O_3$ | | |
| Fe-ETS-4(17) | 0.97 $TiO_2$- 5.89 $Na_2O$- 0.67 $K_2O$- 5.06 $SiO_2$- 115.2 $H_2O$- 0.1 $Fe_2O_3$ | | |
| ETS-4Fe(50) | 0.5 g ETS-4 + 0.05g $FeCl_3$ + 100mL $H_2O$ (ion exchange) | (room temperature) | 6 h |
| ETS-4Fe(25) | 0.5 g ETS-4 + 0.025g $FeCl_3$ + 100 mL $H_2O$ (ion exchange) | | |
| ETS-4Fe(10) | 0.5 g ETS-4 + 0.01g $FeCl_3$ + 100 mL $H_2O$ (ion exchange) | | |

### 2.2.2 Vanadium phosphate experiments

The molar fractions and synthesis conditions for all the synthesized vanadium phosphate samples are listed in Table 2.2. All resulting powders are fine and present a pale green color or green/bluish color.

In the vanadium phosphate synthesis, normally, the phosphorous source $NaH_2PO_4$ (98-100.5 wt.% Riedel-de-Haën) and the vanadium source $VOSO_4.3.55H_2O$ (97 wt.% Aldrich) are dissolved in distilled water as two separate solutions, and stirred for a period of 10 minutes for complete dissolution. The two solutions are then mixed together under stirring, for 40 minutes. In the case of the addition of maleic acid ($C_4H_4O_4$, Carbo Erba) or urea ($CH_4N_2O$, Aldrich), the compounds are added and the mixture is stirred also for 40 minutes in order to obtain a homogeneous solution.

In the case of the use of ethylene glycol ($C_2H_6O_2$, Sigma-Aldrich) or eutectic mixture as solvent, the sources are first dissolved in the desired solvent and then the procedure is similar to the one described above.

The mixtures (or synthesis gels) are then transferred into Teflon-lined autoclaves (in the case of hydrothermal synthesis) or to the microwave vessels (in the case of microwave heating assisted synthesis), and submitted to different periods of time and different synthesis temperatures.

In the case of the use of eutectic mixtures, the mixture was prepared according to literature [7]. The eutectic mixture used in this work, is formed by choline chloride ($C_5H_{14}ClNO$) and urea in a 1:2 ratio. The two components were mixed together under stirring until it becomes a stable liquid (for about 1 day).

**Table 2.2-** Vanadium phosphate compositions and synthesis conditions.

| Sample | Composition (molar fraction) | T (ºC) | Time (days) | Resulting phase |
|---|---|---|---|---|
| VPO_1 | 1.0 $VO_2$ – 6.2 $P_2O_5$ – 46.2 $Na_2O$ – 343.5 $H_2O$ | 170 | 7 d | $Na(VO)(PO_4)$ [1] |
| VPO_2 | 1.0 $VO_2$ – 6.2 $P_2O_5$ – 6.2 $Na_2O$ – 343.5 $H_2O$ - 0.44 urea | | | Unknown 1 |
| VPO_3 | 1.0 $VO_2$ – 6.2 $P_2O_5$ – 6.2 $Na_2O$ – 343.5 $H_2O$ - 0.88 urea | | | Unknown 1 |
| VPO_4 | 1.0 $VO_2$ – 6.2 $P_2O_5$ – 6.2 $Na_2O$ – 343.5 $H_2O$ – 1.77 urea | | | Unknown 1 |
| VPO_5 | 1.0 $VO_2$ – 6.2 $P_2O_5$ – 6.2 $Na_2O$ – 343.5 $H_2O$ – 0.23 maleic acid | | | Unknown 2 |
| VPO_6 | 1.0 $VO_2$ – 6.2 $P_2O_5$ – 6.2 $Na_2O$ – 343.5 $H_2O$ – 0.46 maleic acid | | | Unknown 2 |
| VPO_7 | 1.0 $VO_2$ – 6.2 $P_2O_5$ – 6.2 $Na_2O$ – 343.5 $H_2O$ – 0.92 maleic acid | | | Unknown 2 |
| VPO_8-16 | 1.0 $VO_2$ – 6.2 $P_2O_5$ – 6.2 $Na_2O$ – 343.5 $H_2O$ – 0.92 maleic acid | | 5h, 10h,1-7 d | Unknown 2 |
| VPO_17-18 | 1.0 $VO_2$ – 6.2 $P_2O_5$ – 6.2 $Na_2O$ – 343.5 $H_2O$ – 0.92 maleic acid | | 15 d, 21 d | $Na_3V_2O_2(PO_4)_2F$ [2] |
| VPO_19 | 1.0 $VO_2$ – 6.2 $P_2O_5$ – 6.2 $Na_2O$ – 173.25 $H_2O$ – 49.27 ethylene glycol | | 7 d | |
| VPO_20 | 1.0 $VO_2$ – 6.2 $P_2O_5$ – 6.2 $Na_2O$ – 254.9 $H_2O$ – 24.63 ethylene glycol | | 7 d | |
| VPO_21 | 1.0 $VO_2$- 6.2 $P_2O_5$- 3.2 $Na_2O$- 3.55 $H_2O$ – 5.11 ChCl:urea (eutectic mixture) | | 7 d | |
| VPO_22 | 1.0 $VO_2$- 6.2 $P_2O_5$- 6.2 $Na_2O$- 18.28 $H_2O$ – 5.11 ChCl:urea (eutectic mixture) | | 7 d | $Na_3VO(PO_4)(HPO_4)$ [3] |
| VPO_23 | 1.0 $VO_2$- 6.2 $P_2O_5$- 6.2 $Na_2O$- 33.10 $H_2O$ – 5.11 ChCl:urea (eutectic mixture) | | 7 d | $Na_3VO(PO_4)(HPO_4)$ [3] |
| VPO_24 | 1.0 $VO_2$- 6.2 $P_2O_5$- 6.2 $Na_2O$- 47.87 $H_2O$ –5.11 ChCl:urea (eutectic mixture) | | 7 d | $Na_3VO(PO_4)(HPO_4)$ [3] |
| VPO_25-26 | 1.0 $VO_2$ – 6.2 $P_2O_5$ – 6.2 $Na_2O$ – 343.5 $H_2O$ – 0.92 maleic acid (microwave) | | 1h, 5h | |

[1] K.H. Lii, C.H. Li, T.M. chen, S.L. Wang, *Z. Kristallogr.* 197 (1991) 67; [2] W. Massa, O.V. Yakubovich, O.V. Dimitrova, *Solid State Sciences* 4 (2002) 495; [3] M. Schindler, W. Joswig, W.H. Baur, *Eur. J. Solid State Inorg. Chem.* 32 (1995) 109

### 2.2.3 Microwave heating assisted synthesis

Microwave assisted synthesis experiments were carried out in a CEM microwave oven model Mars 5. The maximum power was 300 W, with a temperature ramp of 10 min, 400 Psi pressure, at a temperature of 170 ºC and for periods of 5 and 10 hours.

## 2.3 Characterization

### 2.3.1 Powder X-ray diffraction (XRD)

Samples were identified by powder X-ray diffraction (XRD) at room temperature in a step-scan regime on an X'Pert MPD Philips diffractometer (CuKα X-radiation) in the 2θ range 5º - 40º.

### 2.3.2 Scanning electron microscopy (SEM)

Scanning electron microscopy was used to analyze the morphology and crystal size of the samples, performed on Hitachi S-4100 and SU-70 microscopes. Also, the relative element ratios analysis was achieved by using energy dispersive X-ray spectroscopy (EDS), carried out by Römteck EDS system attached to the scanning electron microscope.

### 2.3.3 $^{29}$Si MAS NMR

Solid state $^{29}$Si magic-angle spinning (MAS) NMR spectra were collected at 79.49 MHz on a Brucker Avance 400 (9.4 T, wide-bore) spectrometer. Fully hydrated samples were spun at the magic-angle in zirconia rotors. $^{29}$Si MAS NMR

spectra were recorded with 40º pulses, a spinning rate of 5.0 kHz and 35 s recycle delays. Chemical shifts are quoted in ppm from tetramethylsilane (TMS).

### 2.3.4 UV-Visible diffuse reflectance

UV-Vis diffuse reflectance spectra were recorded in air at room temperature, on a JascoV-560 PC spectrometer in the range of 230 – 800 nm using $BaSO_4$ as the reference material.

### 2.3.5 Raman spectroscopy

Fourier-transform (FT) Raman spectra were acquired on a Bruker RFS 100/S spectrometer using a Nd:YAG laser (1064 nm) in the range of 50 – 4000 $cm^{-1}$ with a resolution of 2 $cm^{-1}$ and 400 – 800 scans.

### 2.3.6 Infrared spectroscopy

Fourier transform infrared spectra (FTIR) of powdered samples suspended in KBr pellets were collected in the range of 400 – 4000 $cm^{-1}$ using a Mattson Mod 7000 spectrometer, resolution 2 $cm^{-1}$.

### 2.3.7 Differential scanning calorimetry (DSC)

DSC curves were measured with a DSC-50 Shimadzu analyzer. The samples were heated under air with a rate of 5 ºC/m

# CHAPTER 3
# RESULTS AND DISCUSSION

# 3. Results and Discussion

## 3.1 ETS-4

A pure ETS-4 sample was synthesized in the system 1.0 $SiO_2$ - 0.105 $Na_2O$ - 0.08 $K_2O$ - 0.13 $TiO_2$ - 5.9 $H_2O$. The XRD pattern of the obtained sample is shown in Figure 3.1.

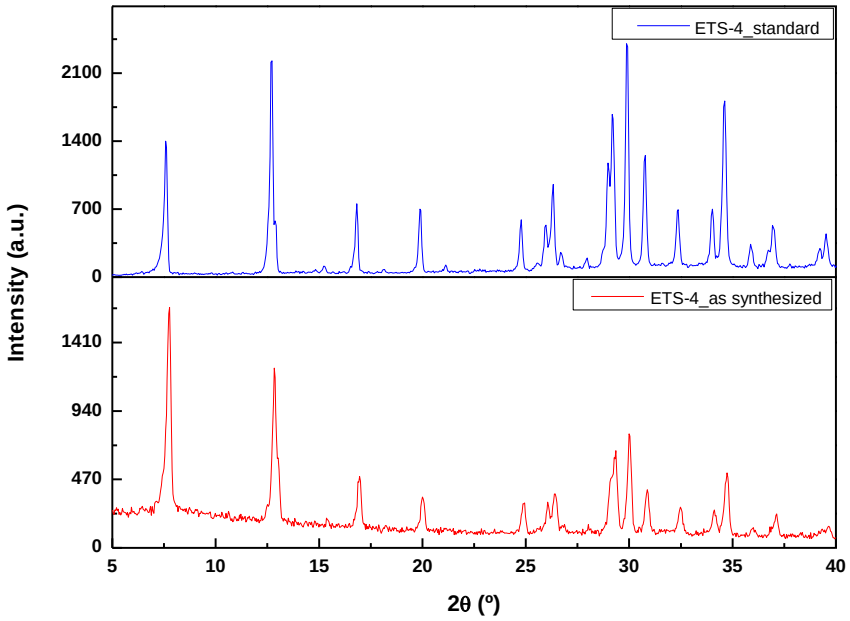


**Figure 3.1-** XRD patterns of the as synthesized ETS-4 sample 1 and of a standard sample.

By comparing the XRD data of the as synthesized sample with the standard one, although there are some differences in the intensity of the peaks, their relative positions are the same, proving the formation of the ETS-4 phase.

An SEM micrograph of the as synthesized sample is presented in Figure 3.2. The sample has a morphology close to the one normally reported to the ETS-4 phase [1]. EDS analysis was also performed, showing silicon to titanium ratio (Si/Ti) of about 2.

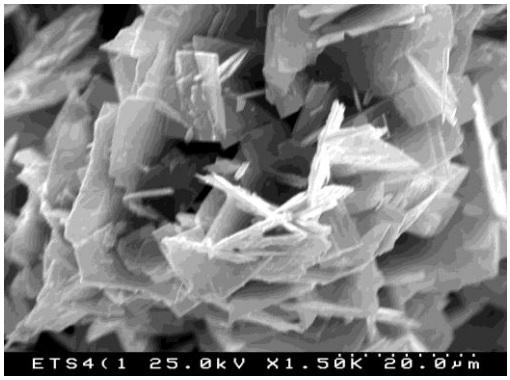


**Figure 3.2-** SEM micrograph of the as-synthesized ETS-4 sample.

### 3.1.1 Fe substitution in ETS-4

Isomorphous substitution in the framework of microporous materials is a route worth to explore since it can provide new materials that show new catalytic, magnetic or other properties, and also, from previously known materials it can modify their properties for certain applications [2].

As mentioned before, because ETS-4 possesses isolated Ti atoms in its structure (mainly isolated titanium atoms in $TiO_5$ square-pyramids), that may be accessible to diffusing/adsorbing species, the substitution of those atoms by others may be interesting. Vanadium and copper are two elements that have already been successfully incorporated into ETS-4 framework [1] [3] [4].

The isomorphous incorporation of iron in the ETS-4 structure is an interesting study, as well as the characterization of the resulting products. Besides, zeolite-like structures containing iron are very useful catalysts in several reactions, for example, $NO_x$ [5]-[8] decomposition and selective of benzene to phenol [9] [10].

In order to study the possibility of the replacement of titanium (Ti) by iron (Fe) in the ETS-4 structure, isomorphous substitution experiments were carried out. The iron substitution can be of importance because it may give novel properties to ETS-4, mainly magnetic ones. A combination of different techniques and experiments were used to study the inclusion of Fe in ETS-4 material.

Different percentages of Ti in the synthesis gel were replaced by iron using iron chloride ($FeCl_3$). Samples with 5, 9, 13 and 17 mol % of iron replacing titanium were synthesized hydrothermally, giving samples Fe-ETS-4(x), where x is the molar percentage of iron used to replace titanium in starting gel (Table 2.1). The resulting XRD patterns are depicted in Figure 3.3.

The diffraction patterns of all Fe-ETS-4(x) samples are very similar to the one of the ETS-4 sample. All reflections from ETS-4 phase are clearly seen, indicating the successful synthesis of ETS-4 from gels containing different amounts of $FeCl_3$.

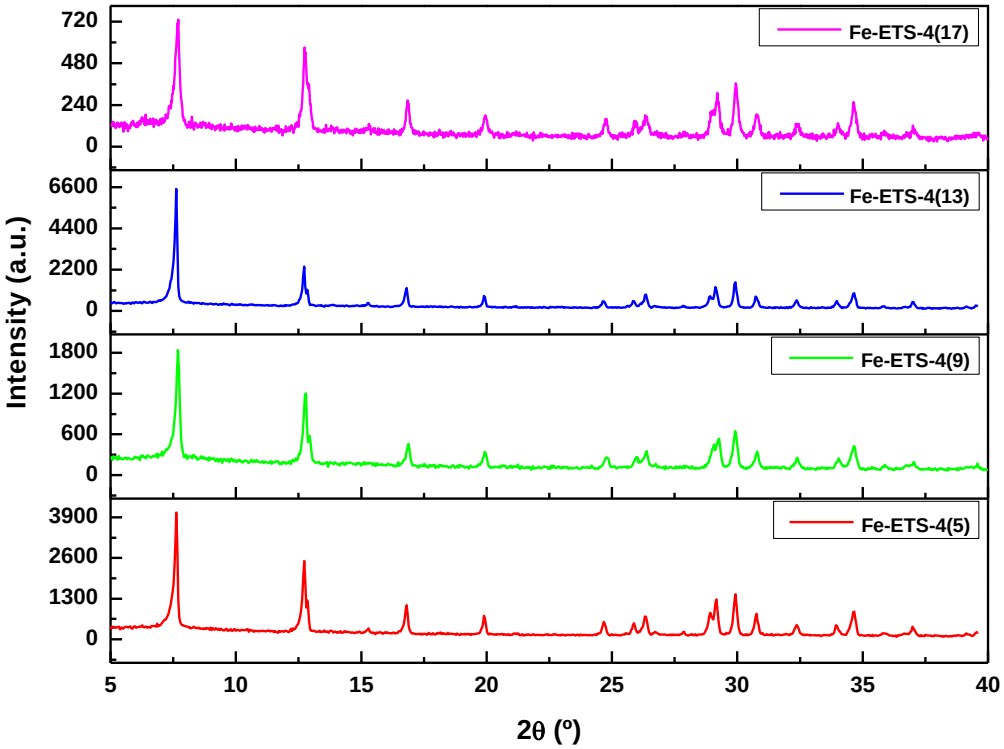


**Figure 3.3-** XRD patterns of the Fe-ETS-4(5), Fe-ETS-4(9), Fe-ETS-4(13), Fe-ETS-4(17), respectively.

The XRD patterns are not very distinct from the one of standard ETS-4, except for sample Fe-ETS-4(17) that has a small extra peak at 2θ 6.3º. No other crystalline phases were identified.

The unit cell parameters for ETS-4 and Fe-ETS-4(x) samples were refined in orthorhombic space group *Cmmm* (No. 65) (ETS-4: *a*= 23.240, *b*= 7.191, *c*=6.961 Å, *V*= 1163.3 Å$^3$; and Fe-ETS-4(5-13): *a*= 23.220-23.257, *b*= 7.203-7.213, *c*= 6.964-6.984 Å, *V*= 1166-1170 Å$^3$). According to these results, the unit cell parameters are quite similar, indicating that no significant structural changes occurred for Fe-ETS-4 materials. So the increase of the iron content does not influence the obtained phase.

SEM/EDS (Scanning Electron Microscopy/Energy Dispersive Spectroscopy) analysis was performed in order to study the crystal morphology and to prove the presence of iron in the ETS-4 samples.

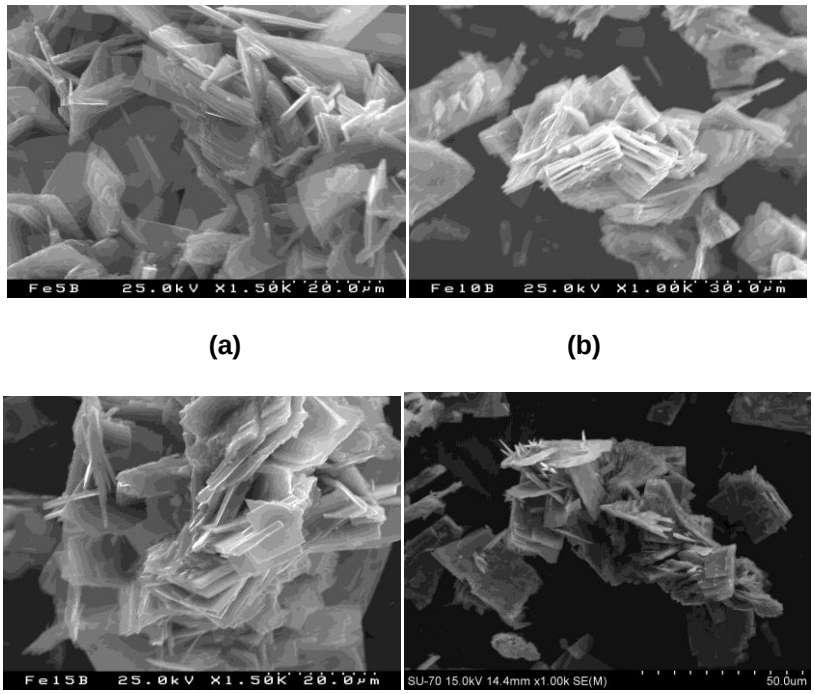


**(a)** **(b)**

**(c)** **(d)**

**Figure 3.4-** SEM images of **(a)** Fe-ETS-4(5), **(b)** Fe-ETS-4(9), **(c)** Fe-ETS-4(13) and **(d)** Fe-ETS-4(17).

From the SEM images in Figure 3.4, it can be seen that for the different percentages of iron added to the synthesis gel, the morphology of the obtained crystals is very similar. All the samples are well crystallized and have similar

morphology, being aggregates composed of plate crystallites. The morphology of the Fe-ETS-4(x) samples does not change with the amount of iron in the precursor gel. X-ray mapping was also performed, and the results are presented in Figure 3.5.

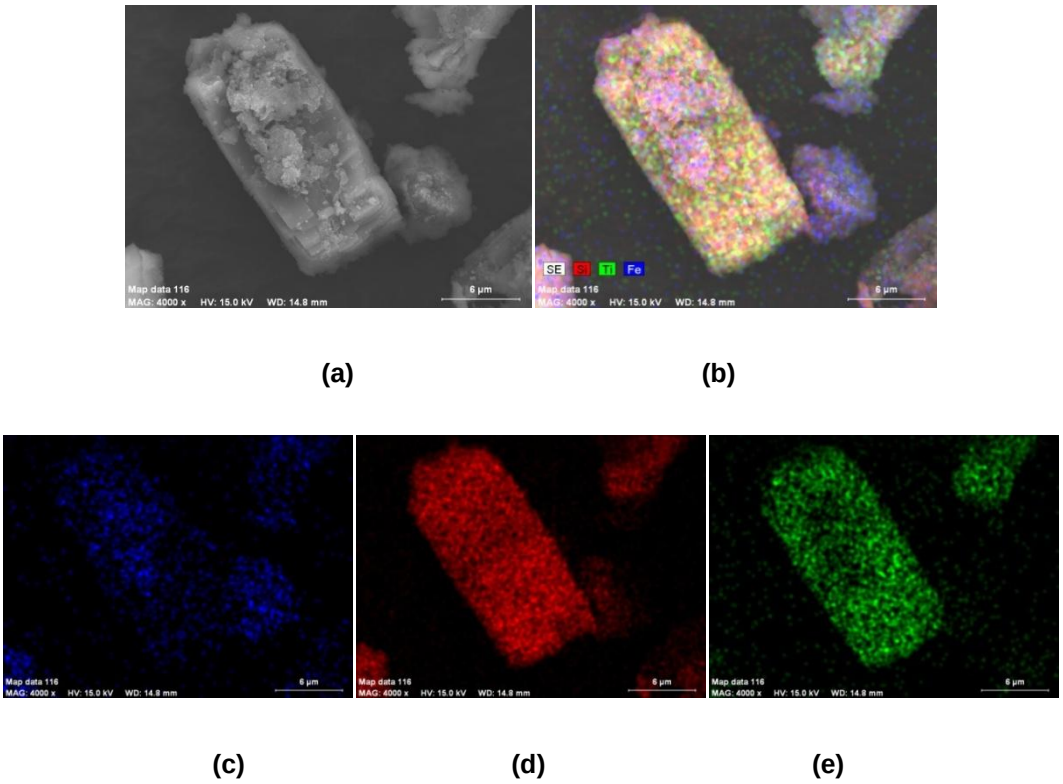


**Figure 3.5-** X-ray mapping images for the sample Fe-ETS-4(17); **(a)** the normal SEM micrograph **(b)** x-ray mapping picture, with all three elements, Fe, Si and Ti **(c)** distribution of Fe **(d)** distribution of Si **(e)** distribution of Ti.

The crystal under study (Fe-ETS-4(17)) is rich in both Si and Ti elements, as expected, but also shows the presence of Fe element, although in less quantity and also possibly located only on the surface of the crystal. These x-ray mapping images are used to illustrate the element distributions of a crystal, but cannot be used to calculate relative element ratios, because the topographic effects may also influence the images and the results, since the crystal surface is not very regular.

EDS of selected area of the sample Fe-ETS-4(17) (Figure 3.6) shows the presence of low quantity of iron in the sample.

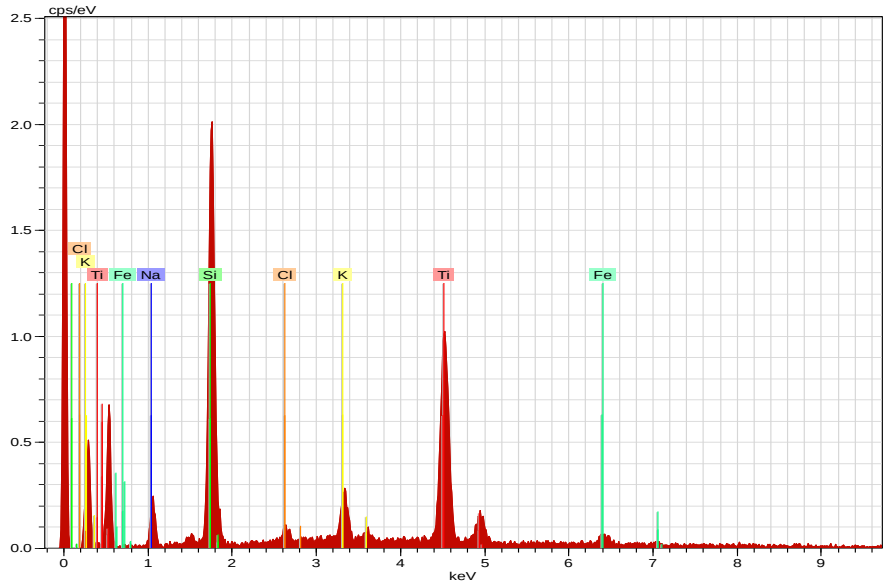


**Figure 3.6-** EDS results for the sample Fe-ETS-4(17).

The Si/Ti, Fe/Ti and Si/(Ti+Fe) ratios obtained from EDS for different Fe-ETS-4(x) samples, performed in a number of particles, are listed in table 3.1, showing the different amount of Fe in Fe-ETS-4(x) samples.

These SEM and EDS results of a number of particles prove the presence of Fe in the Fe-ETS-4(x) samples, showing that they contain Ti and Fe. For both Fe-ETS-4(5) and Fe-ETS-4(9) samples, the relative Si/Ti ratio seems to be in accordance with what is expected for ETS-4, with exception of the Fe-ETS-4(17) sample that presents a higher value. These results show that the incorporation of Fe in the ETS-4 is limited, since the increase of Fe in the gel does not result in a directly proportional higher Fe/Ti ratio of the final sample.

**Table 3.1-** The Si/Ti, Fe/Ti and Si/(Ti+Fe) ratios obtained from EDS.

| Sample | Si/Ti | Fe/Ti | Si/(Ti+Fe) |
|---|---|---|---|
| Fe-ETS-4(5) | 2.0 | 0.025 | 1.9 |
| Fe-ETS-4(9) | 2.1 | 0.090 | 2.0 |
| Fe-ETS-4(13) | 1.9 | 0.0773 | 1.7 |
| Fe-ETS-4(17) | 2.9 | 0.125 | 2.6 |

### 3.1.2 Ion exchange in ETS-4

Ion exchange experiments were carried out with a pure ETS-4 sample, in order to be able to compare results. When preforming ion exchange for microporous materials, the cations or species contained or held electrostatically in the pores of the material will be exchanged with the other cations in an electrolyte solution that is put in contact with the porous material.

By carrying out the ion exchange of ETS-4 with Fe in a $FeCl_3$ solution, we know for sure that the Fe ions are located in the pores of the ETS-4 structure. This can be very useful to compare results with as synthesized samples and to speculate on the location of iron in the as synthesized samples. The XRD results for Fe exchanged ETS-4 are presented in Figure 3.7.

The XRD pattern is the same as the one obtained for pure ETS-4 sample, proving that the ETS-4 phase is maintained and that ion exchange does not influence the structure of the material. Unit cell parameters are similar to the ones reported for as-synthesized samples with Fe, meaning that no major structural changes occur after ion exchange.

EDS results give an Fe/Ti ratio of about 0.066 for sample ETS-4Fe(50) and about 0.03 for the sample ETS-4Fe(25), clearly different values than the ones obtained for as synthesized samples.

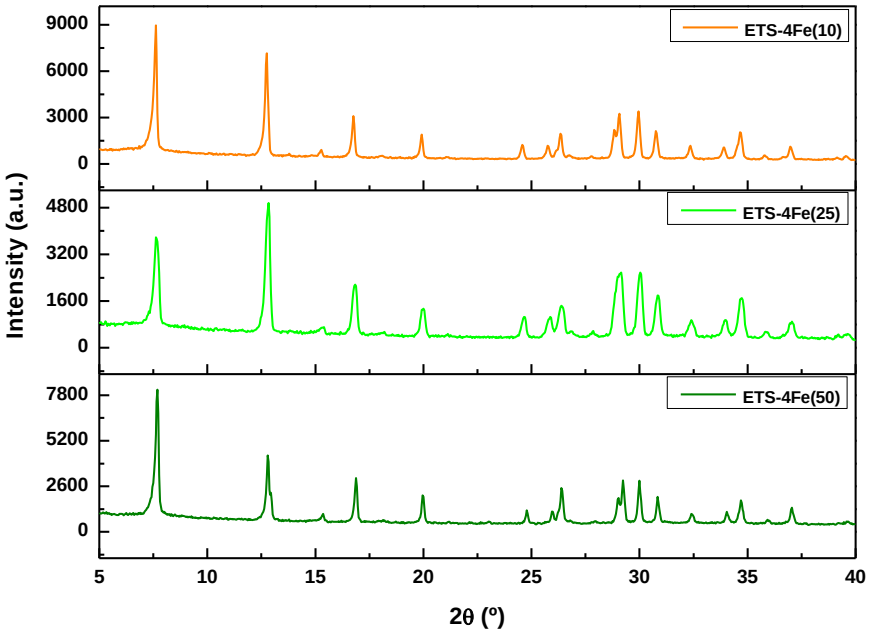


**Figure 3.7-** XRD results for the samples resulting from Fe exchange in different amounts, 0.01 g, 0.025 g and 0.05 g of $FeCl_3$, and 0.5 g of pure ETS-4 powder in water, giving samples ETS-4Fe(50), ETS-4Fe(25) and ETS-4Fe(10).

During this ion exchange experiments, when washing the powdered sample, it was noticed that the washing water was orange instead of colorless, normal for previous experiments. This can mean that the iron was possibly washed away of the samples, and that could be the reason for a lower Fe/Ti ratio.

### 3.1.3 DR UV-Vis experiments

Diffuse Reflectance UV-Visible (DR UV-Vis) spectra are normally very useful and reliable to detect the presence of framework or extra-framework metal

species in porous materials [1], since their presence can be detected by subtle alterations or shifts in the peaks of the spectra.

When transition metal ions are substituted in the framework of molecular sieves, charge transfer (CT) transitions occur between the transition metal ions and the framework oxygen anions [11]. Normally those transitions occur in the UV region. DR UV-Vis spectra of the as synthesized samples of ETS-4, Fe-ETS-4(x) and a sample obtained by ion exchange were recorded. Results are presented in Figure 3.8.

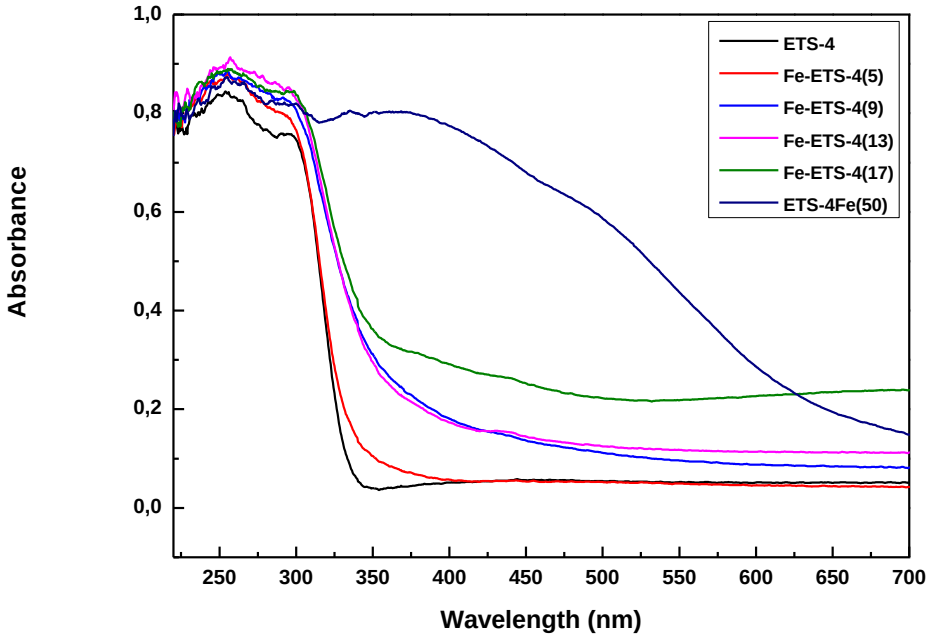


**Figure 3.8-** DR UV-Vis spectra for samples ETS-4, Fe-ETS-4(x) and ETS-4Fe(50).

ETS-4 DR UV-Vis spectrum presents two characteristic peaks at around 250 nm and 290 nm that are due to the $O^{2-} \rightarrow Ti^{4+}$ CT transitions that occur along the Ti-O-Ti chains [1]. The peak at ca. 250 nm results from the delocalized charge transfer transitions along the Ti–O–Ti chains and the one at ca. 290 nm is due to defect states within the band gap formed by the interruption of Ti–O–Ti chains [1].

For all the analyzed Fe-ETS-4(x) samples, the DR UV-Vis displays those two peaks at ca. 250 and 290 nm, revealing no major structural alterations.

According to literature [11] [12] when Fe-O-Si bonds are present in a structure of this type (silicate based, zeolite like), a CT transition between the O of tetrahedra and $Fe^{3+}$ atoms in the framework is observed around 250 nm, producing an adsorption band in the spectrum. In the spectra of the analyzed samples (Figure 3.8), that band is not visible, possibly due to the overlapping of the bands resulting from the titanium to oxygen CT and iron to oxygen CT transitions (since they occur at very close wavelengths, as denoted in Figure 3.9). This is not surprising, since it has been reported that Fe(III) containing silicates have been studied previously using UV-Vis spectroscopy [13], and according to that, bands below 340 nm are overlapped with those from Ti(IV) in different states. CT bands of Fe(III) are red-shifted with increasing number of coordinating oxygen ligands, giving band at ca. 290 nm for isolated Fe(III) in octahedral coordination.

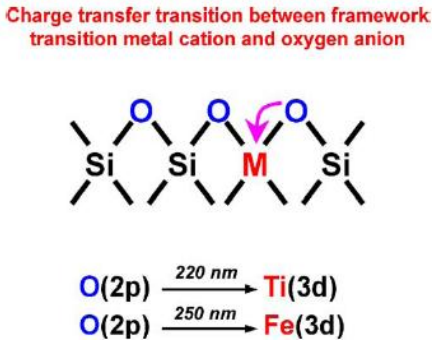


**Figure 3.9-** Transition metal ions in silicate frameworks and charge transfer (CT) transitions between metal cations M (in this case Ti and Fe) and oxygen anion and their characteristic wavelengths (UV region) [11].

Previous studies indicate that $Fe_2O_3$ crystallites are responsible for bands around 500 and 670 nm [14], FeO(OH) and calcined FeO(OH) show strong maxima at 535 and 515 nm, respectively [15], and bands between 300-400 nm may be due to octahedral Fe(III) in small oligomeric $Fe_xO_y$ clusters [16].

The spectra on Figure 3.8 show that the absorption edge is red-shifted with increasing Fe content of the Fe-ETS-4(x), which shows that Fe ions become near

with higher Fe content. This is in accordance with the observation that those as-synthesized samples Fe-ETS-4(x) are no longer the white powder, typical for ETS-4, but rather a light yellowish brown powder, normal for Fe-containing materials.

The spectrum for the ion exchanged sample, ETS-4Fe(50), shows significant absorption in the region between 340 and 600 nm, which probably indicates the formation of iron oxide particles, which is in accordance with the observation of the dark orange color of the ETS-4Fe(50) samples. The absorbance of this sample happens for a broad range of wavelength, and suggests the existence of several different small $Fe_xO_y$ clusters to larger $Fe_2O_3$ species.

Taking into account the above said, the absence of broad bands in the visible region for samples Fe-ETS-4(5-9) reveals that there are no $Fe_2O_3$ species in those samples. On the other hand, sample Fe-ETS-4(17) clearly has absorption in the visible region, meaning that probably has iron oxide particles.

Sample Fe-ETS-4(13) has weak absorption at ca. 440 nm, and close inspecting sample Fe-ETS-4(17) reveals also weak absorption at that wavelength, though the origin of that absorption is not clear. Previous studies [17] [18], suggest that tetrahedral coordinated Fe(III) species will give absorptions bands at 375, 410, 440 and 480 nm, assigned to d-d forbidden transitions. In ETS-4, Ti atoms are present in pentahedral or octahedral coordination, and silicon atoms present tetrahedral coordination, being that all Si atoms are involved in Si-O-Ti bonds. If Fe(III) substitutes Si atoms, the net charge of the ETS-4 framework would increase, altering its stability. Since, to date, there are no reports of isomorphous substitution of Si by other M(III) ions, most probably this weak absorption band (ca. 440 nm) is due to the presence of $Fe_xO_y$ clusters in the ion exchanged sample.

### 3.1.4 Infrared/Raman experiments

Since Infrared (IR) and Raman are sensitive to the chemical environment of the atoms in a certain framework or structure, these types of experiments can be useful for the possible identification of iron in the ETS-4 structure. In this case, spectra of the as synthesized samples, Fe-ETS-4(x), are compared with spectra of pure ETS-4 and with spectra collected from ETS-4Fe(50) sample. Results are presented in Figures 3.10 and 3.11.

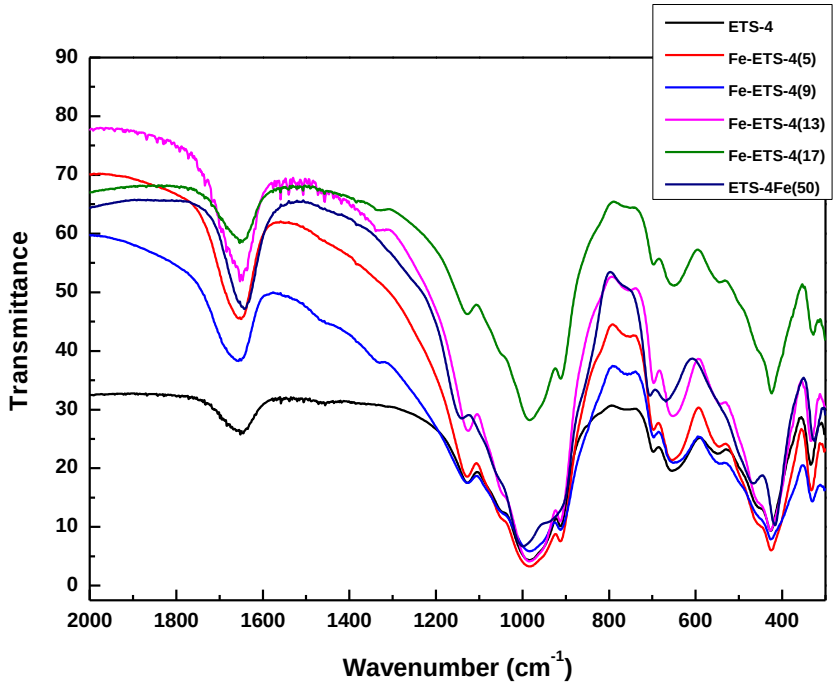


**Figure 3.10-** IR spectra for samples Fe-ETS-4(x) and ETS-4Fe(50).

As it has been previously mentioned, ETS-4 structure is built up of chains of corner-sharing [$TiO_6$] octahedral along the b direction, which are laterally linked by [$SiO_4$] tetrahedral, constructing two orthogonal sets of channels [19]. So, two systems of atoms can be considered in this structure, to facilitate IR and Raman spectra analysis; a silicon-oxygen system where the atoms are arranged in 8MRs tethrahedra, and a titanium-oxygen system in which the atoms are arranged in

pyramids and in chains of octahedral [1] (revealing the two different coordination geometries of Ti atoms, square-pyramidal and octahedral), that present characteristic vibrations at defined frequencies in the spectra.

ETS-4 IR spectrum in Figure 3.10 seems to be in close agreement to previously tabled results for this structure [20]. Spectrum presents a strong peak at ca. 1000 $cm^{-1}$, referring to Si-O stretching mode. A split peak of less intensity in the 700 $cm^{-1}$ region is probably due to Ti-O stretching mode and possibly O-Ti-O and Ti-O-Ti bending modes. The peaks that appear for frequencies around 550 $cm^{-1}$ can possibly be assigned to O-Si-O, Si-O-Si and O-Ti-O bending modes, as well as Si-O-Ti asymmetric and symmetric stretching modes and the rocking mode. The peaks around 1650 $cm^{-1}$ are normally attributed to typical vibrations in water molecules.

There are not many apparent differences between ETS-4 IR spectrum and the other spectra, meaning that no major structural alterations are observed in samples with Fe (both as synthesized and ion exchanged).

In previous studies on incorporation of transition metal ions (M) in molecular sieves [12], the peak around 1000 $cm^{-1}$ presented shifts along with the increase of M content. That peak corresponds to characteristic stretching vibrations of tetrahedral $SiO_4$ units, and so, shifts may indicate that heteroatoms are incorporated in the framework and M-O-Si bonds are formed. If the M specie is located in the surface of the structure, IR could also prove that presence, since the bending vibration of surface Si-O (apical bonds) around 450 $cm^{-1}$ would also be shifted [12]. Interestingly, the FTIR spectrum of the ion exchanged sample, ETS-4Fe(50), shows shifts for almost all peaks. Although the origin of this shift is not clear, this result indicates that the Fe is not located in the pores of the ETS-4 structure for Fe-ETS-4(x) samples.

Raman spectra (Figure 3.11) of the as synthesized ETS-4 and Fe-ETS-4(x) are very similar, no new bands appeared when Fe has been incorporated.

The typical Raman spectrum for ETS-4 has a split peak between 1100 and 1000 $cm^{-1}$ due to asymmetric stretching of Si-O-Si bridges. It also presents peaks around 910 and 960 $cm^{-1}$ that correspond to Si-O stretching, and also an intense peak around 750 $cm^{-1}$ attributed to Ti-O-Ti symmetric stretching. Peaks in the 800-900 $cm^{-1}$ region can be also identified corresponding to stretching of shorter, apical bonds in $TiO_5$ units (Ti in square-pyramidal coordination). Peaks for lower frequencies 500-400 $cm^{-1}$ are not very clear since the assignment of this region is not yet fully understood [1].

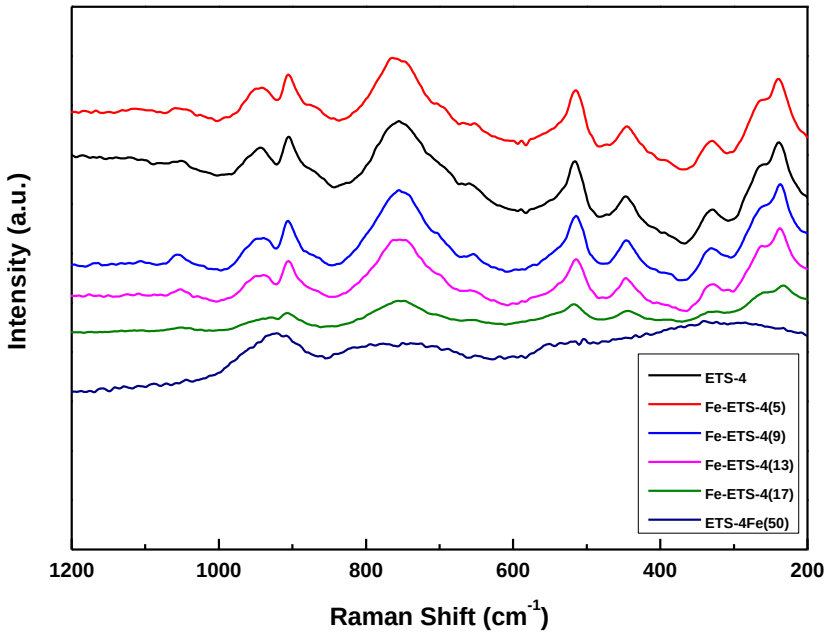


**Figure 3.11-** Raman spectra of samples ETS-4, Fe-ETS-4(x) and ETS-4Fe(50).

The Raman spectra presented in Figure 3.11 seems to be in agreement with the ETS-4 typical Raman spectrum, therefore, not showing direct evidence of Fe introduction in the ETS-4 framework. In a previous work by Li [11], where Fe was incorporated in a molecular sieve structure, the resulting Raman spectrum presented bands around 500 $cm^{-1}$ corresponding to Fe-O-Si isolated species

stretching/bending vibrations, and also bands between 1000-1200 $cm^{-1}$ due to Fe-O-Si stretching vibrational modes. Those peaks are not clearly seen in the experimental Fe-ETS-4(x) results, and thus not giving direct evidences about Fe incorporation in the ETS-4 structure.

### 3.1.5 Differential Scanning Calorimetry (DSC) experiments

DSC experiments were also carried out with ETS-4 samples, in order to study the influence of Fe on the thermal stability of ETS-4. Results are depicted in Figure 3.12.

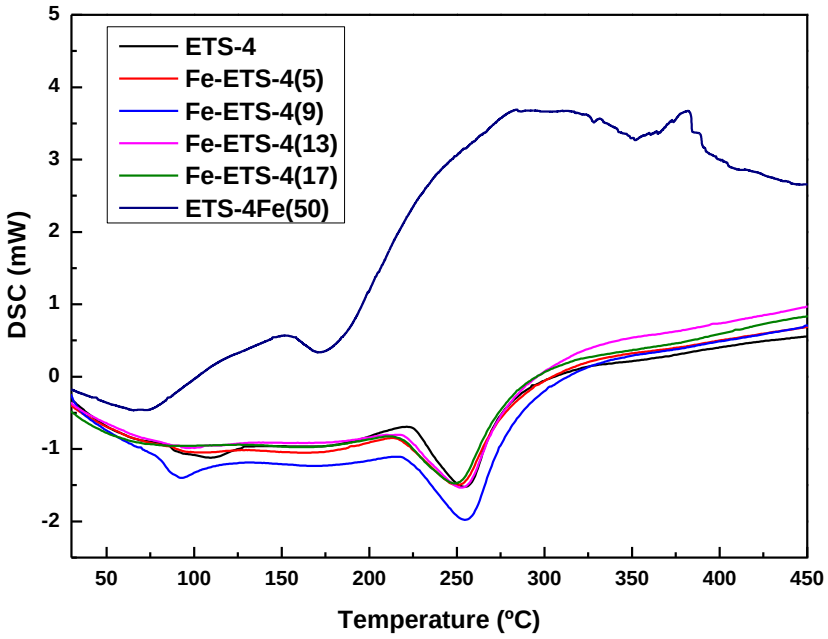


**Figure 3.12-** DSC results for ETS-4 samples, pure, with different percentages of Fe added to the synthesis gel and ion exchanged one.

All DSC curves of ETS-4 and Fe-ETS-4(x) samples appear to be very similar, presenting one endothermic peak at approximately 250 ºC, that according to literature [11] refers to the loss of structural water. These water molecules participate in the construction and maintenance of structural integrity of the

framework, since the interaction of the $TiO_5$ pyramidal species in ETS-4 structure is made through water molecules, making them part of the structure [19]. This endothermic peak determines the thermal stability of materials with ETS-4 structure and means that is at this temperature that structural water is removed from the ETS-4 structure. Alterations in this peak, or in the temperature for this structural water removal, mean structural changes and can indicate presence of different species.

Close inspecting the endothermic peaks shows the small shift in only 5 ºC. It's known that the temperature at which the structural water is removed depends on the nature of the non-framework and exchangeable cations incorporated in the structure. If Fe atoms (cations) of the Fe-ETS-4(x) samples is by any chance located in the pores, that may be responsible for this shift in the endothermic peak.

Another, weaker, endothermic peak is noticed around 100 ºC, that can be referent to the release of water occluded in the pores of the ETS-4 structure.

DSC results for the ion-exchanged sample, ETS-4Fe(50) shows an alteration in the peaks position, being a shift for lower temperatures (of about 75 ºC), which reveals loss of thermal stability for this sample. This is something that was expected, since the sodium cations, involved in the stable structure of ETS-4 are exchanged by iron cations, with different cation radius and charges, which can cause alterations in the maintenance of ETS-4 structure, while submitting it to heating.

### 3.1.6 $^{29}$Si MAS NMR experiments

Nuclear Magnetic Resonance (NMR) is probably one of the most powerful techniques for structural analysis, since it is very sensitive to the chemical environment of the nucleus under study.

To evaluate possible structural alterations of the structure under study, solid state $^{29}$Si MAS NMR spectra of ETS-4, Fe-ETS-4(x) and ETS-4Fe(50) were recorded and are presented in Figure 3.13.

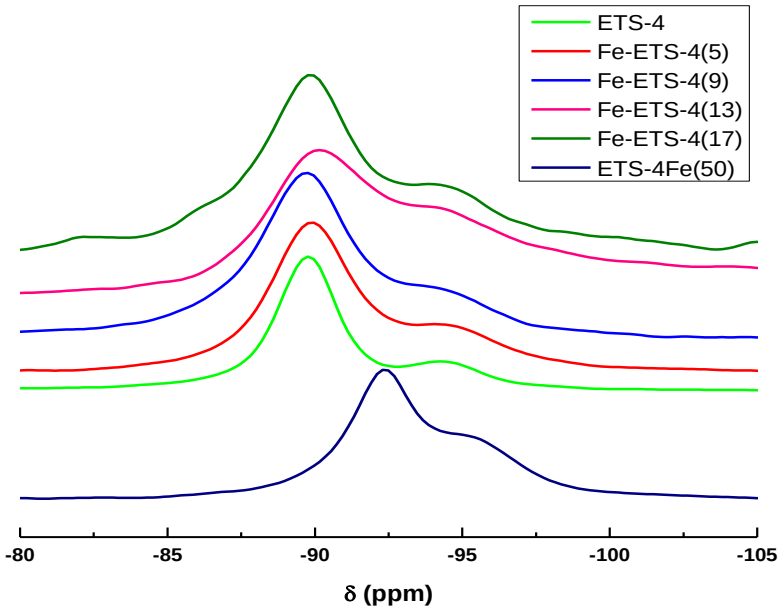


**Figure 3.13-** $^{29}$Si MAS NMR spectra of sample ETS-4, Fe-ETS-4(x) and ETS-4Fe(50).

Normally, ETS-4 $^{29}$Si MAS NMR spectrum presents a strong peak around -90 ppm and another weaker one at -94.5 ppm [21]. These two peaks indicate that, in ETS-4, silicon atoms are in two different environments, and this is clear since Si atoms may be linked in two different manners and with titanium atoms with different coordination geometries Si(2Si,2M) and Si(3Si,M) (where M is Ti atom) as exemplified in Figure 3.14, Si-O-Ti(octahedral) connection type and Si-O-Ti(square-pyramidal) type, that are in agreement with the structural features of ETS-4 [6] that have been previously discussed. The replacement of an atom in the structure (as for example replacement of Ti by Fe), would implicate new connections/"bridges" between the atoms that form the framework, and that would be revealed by shifts in the resulting NMR spectrum.

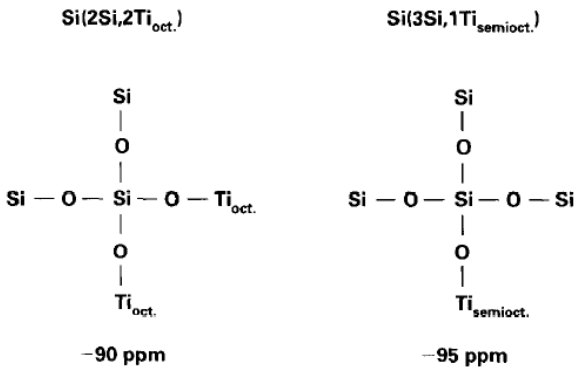


**Figure 3.14-** Examples of the two different chemical environments for Si atoms in ETS-4 structure associated with the different coordination geometries of Ti atoms [21].

For all as synthesized samples, Fe-ETS-4(x), the spectra are clearly broadened when comparing with the ETS-4 spectrum, and the resonance at -94.5 ppm becomes a shoulder with increasing incorporation of iron. The spectra of Fe-ETS-4(13-17) also shows a much broader signal between -80 and -100 ppm, which is expected since Fe(III) ions are paramagnetic. When paramagnetic centers are incorporated into a silicate framework, the $^{29}$Si MAS NMR spectrum is usually broadened and the spin side bands increase significantly. This may suggest that the Si nuclei neighboring Fe(III) eventually give very broad signal in the $^{29}$Si MAS NMR spectrum, which is similar to previous work, where vanadium was incorporated in ETS-4 structure [1].

Table 3.3 represents the intensity ratios between the two peaks of ETS-4 and Fe-ETS-4(x). Ratios are in close agreement with previous reports that gave this ratio between 3:1 and 10:1 [22].

According to the already discussed ETS-4 structure [21], Si(2Si,2M) connects to the $MO_6$ and Si(3Si,M) connects to $MO_5$. The evolution of the intensity ratio of the two resonances could be related to the preferential position that Fe ions may substitute; if Fe substitutes $MO_6$ site, resonance at ca. -90 ppm should decrease. With different amounts of Fe added in the synthesis precursor gel, the

preferential position for Fe seems to be different. Changes of the intensity ratio can also be due to different defect content in ETS-4 and Fe-ETS-4(x).

**Table 3.2-** Intensity ratios of the two typical ETS-4 resonances, for ETS-4 and Fe-ETS-4(x) sample.

| Resonance (ppm) | ETS-4 | Fe-ETS-4(5) | Fe-ETS-4(9) | Fe-ETS-4(13) | Fe-ETS-4(17) |
|---|---|---|---|---|---|
| -90 | 88 | 74 | 84 | 85 | 76 |
| -94.5 | 12 | 26 | 16 | 15 | 24 |

On the other hand, the $^{29}$Si MAS NMR spectrum for sample ETS-4Fe(50), shows a ca. 2.5 ppm upfield shift in peak position. This results show definite proof that in Fe-ETS-4(x) samples, the Fe atoms are not located in the pores of the structure, because if they were, resonances of the $^{29}$Si MAS NMR spectra would also shift upfield, like in the spectrum for the ion exchanged sample

This observation, together with the identification of iron in the samples through EDS chemical analysis, strongly suggests that iron is really present in the framework of as synthesized Fe-ETS-4(x) samples. Although the location of the Fe atoms is not exactly known, it is now clear that they are not in the pores as charge compensator.

## 3.2 Vanadium Phosphates

Vanadium phosphates are interesting materials from commercial and structural point of view. They are known mainly for their catalytic and magnetic properties. Although vanadium phosphates have been studied intensively the

preparation of new material is still possible because the synthesis in this system is very sensitive to the experimental conditions. The previous work of Ferdov *et al.* [23] is an example of a new sodium vanadium (III) phosphate phase synthesized with MPMD, which displays magnetic properties and is described as being very sensitive to experimental conditions.

Several vanadium (III) phosphates have been reported. Phases $VPO_4$ and $V(PO_3)_3$ were synthesized at high temperatures [24] [25], and $VPO_4.H_2O$ and $V_{1.23}(PO_4)(OH)_{0.69}(H_2O)_{0.31}.0.33H_2O$ were hydrothermally prepared by reduction of $V_2O_5$ with V metal in the presence of $H_3PO_4$ and organic amine [26]. $VPO_4.H_2O$ material was also synthesized from $V_2O_5$ and $H_3PO_4$ in the presence of tripropyl amine, which also acted as a reducing agent [27]. A different phase, $H_3OVP_2O_7$ was prepared hydrothermally in the presence of tetraethyl ammonium chloride [28]. These vanadium (III) phosphate phases can also be used as starting reagents for vanadium phosphate glasses or catalysts. These show how different experimental conditions result in different phases and products, that belong to the same family of materials.

As already mentioned in the introduction, the formation of $Na_3V(OH)(HPO_4)(PO_4)$ was extremely sensitive to the synthesis condition. In other word, this system may originate new crystalline phases at slight different synthesis conditions. The starting molar composition in this study is close related to the one for the synthesis of $Na_3V(OH)(HPO_4)(PO_4)$.

Initially, a vanadium phosphate sample without organic additives, VPO_1 sample, was synthesized and the XRD pattern of the obtained product is depicted in Figure 3.15. The product of the hydrothermal synthesis was a fine pale green powder, possibly indicative of V(IV) presence. XRD analysis indicated that instead of $Na_3V(OH)(HPO_4)(PO_4)$ the compound is sodium oxovanadium phosphate(V), $Na(VO)(PO)_4$.

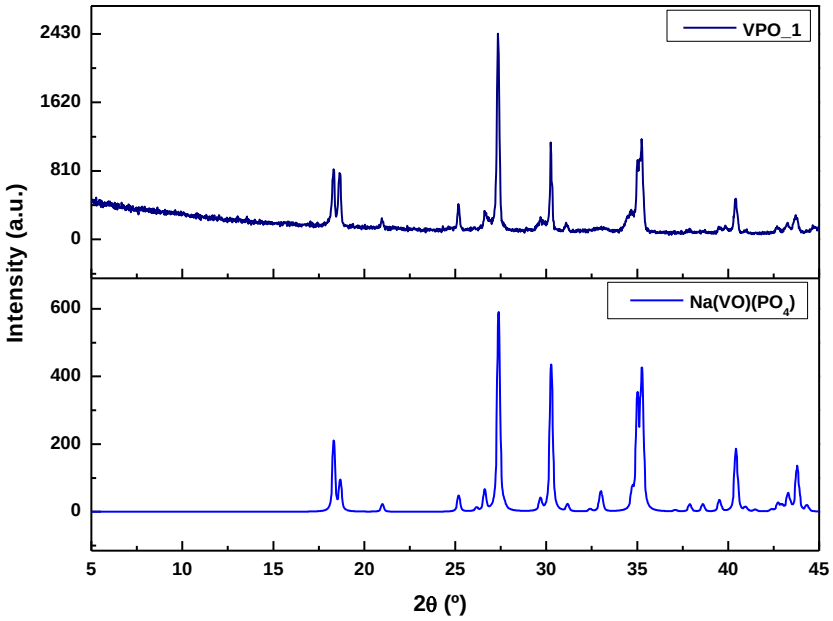


**Figure 3.15-** XRD pattern of VPO_1 sample synthesized without additives, and calculated pattern of $Na(VO)(PO_4)$.

SEM micrographs of this sample (in Figure 3.16) allow to see the morphology and size of the resulting crystals, showing polycrystalline particles with about 50 μm constituted by intergrowth of smaller crystals. EDS analysis confirms the existence of both vanadium and phosphor in a ratio near 1.

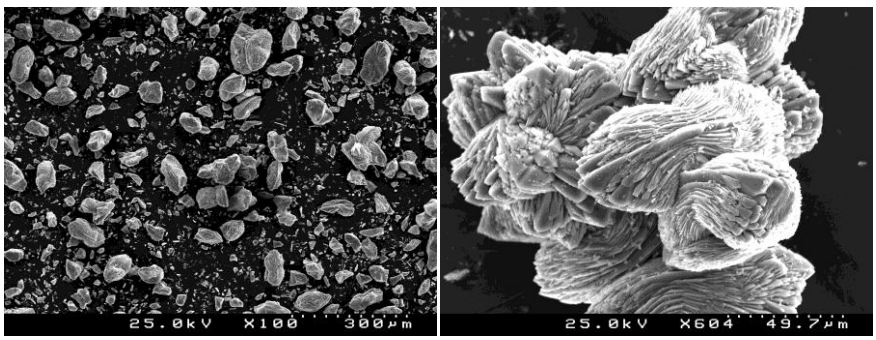


**Figure 3.16-** SEM images of VPO_1 sample.

### 3.2.1 Addition of urea and maleic acid

In order to study the influence of organic additives on the formation of vanadium phosphate phase, the previous experience was repeated using the same molar composition of Na, V(IV), P and water, but with the addition of different amounts of two compounds, urea and maleic acid (Figure 3.17).

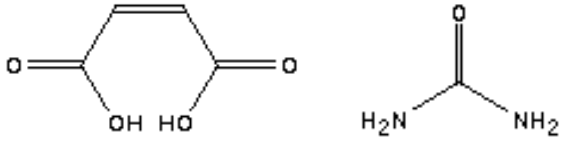


**Figure 3.17-** The maleic acid (left) and urea (right) [29],[30].

Since maleic acid is a dicarboxilic acid while urea is a slightly basic compound and both may reduce vanadium, they were chosen as organic additives. They were added to the precursor mixture to study if different crystalline phases with low vanadium valence can be formed. It is also important to notice that, urea can decompose into ammonium at high temperatures, and that ammonium cations can also play the role of template or structure directing agents in the synthesis.

XRD patterns of the different obtained samples are presented in Figures 3.18 and 3.19.

From the XRD results, it is obvious that the presence of urea and maleic acid influences the formation of vanadium phosphate phases, since the crystalline product is different from the previously reported one ($NaVOPO_4$). Also, urea and maleic acid produce different crystalline phases, probably due to the chemical characteristic of the additives and the different synthesis conditions that they create.

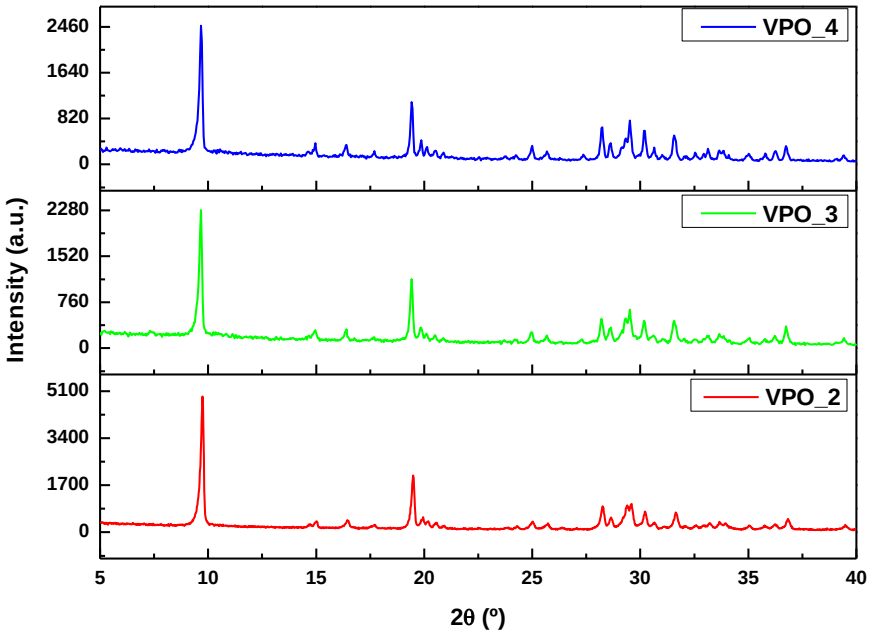


**Figure 3.18-** XRD patterns of samples synthesized with different amounts of urea (VPO_2, VPO_3 and VPO_4).

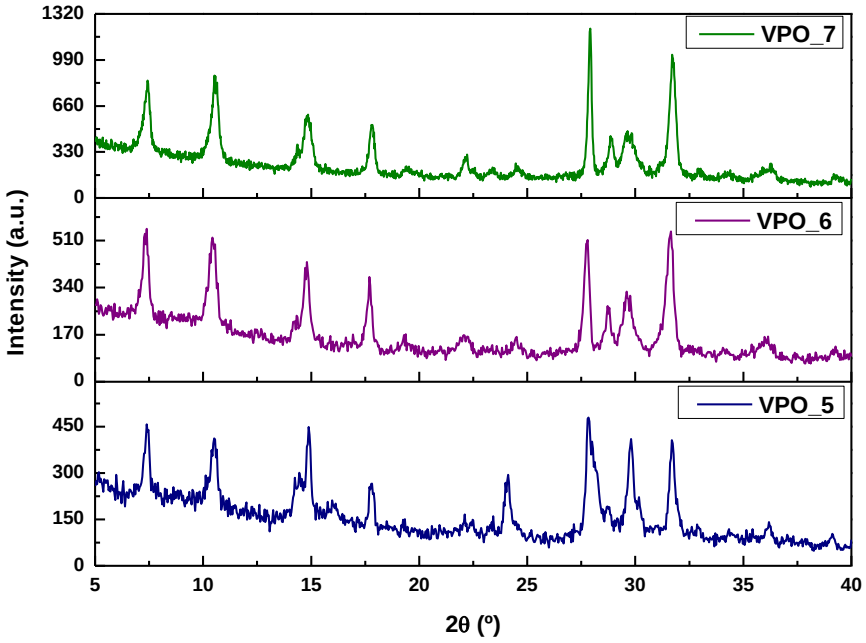


**Figure 3.19-** XRD patterns of samples synthesized with different amounts of maleic acid (VPO_5, VPO_6 and VPO_7).

In the case of urea addition, the XRD diffractograms are the same for different amounts added to the precursor solution, although intensity of the peaks is higher for lower urea content, indicating higher crystallinity.

The XRD patterns are also the same when different amounts of maleic acid were added. The peak positions are approximately the same for all three samples, but intensity is higher for sample with highest amount of maleic acid.

From XRD database, no compound with such kind of XRD patterns can be found. The XRD search-match also does not suggest they are mixture. The index of the both patterns gave triclinic symmetry. In this case, further studies are needed to confirm the phase purity. SEM images of this phase were also obtained (Figure 3.20 and 3.21).

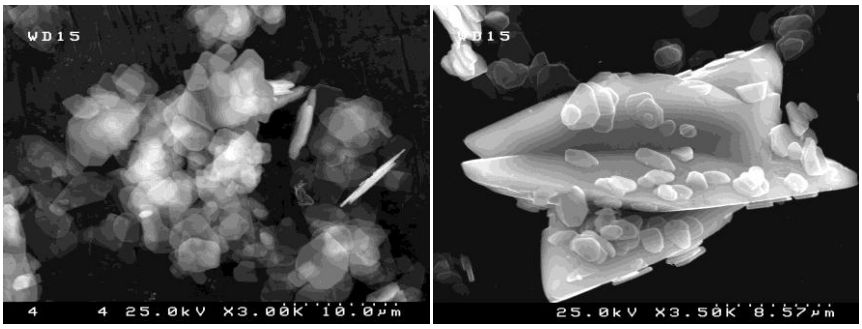


**Figure 3.20-** SEM images of samples synthesized with the addition of urea (VPO_3, left and VPO_4, right).

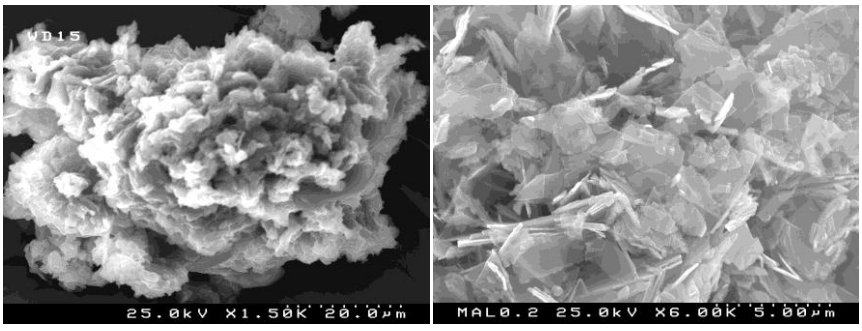


**Figure 3.21-** SEM images of samples synthesized with the addition of maleic acid (VPO_6, left and VPO_7, right).

SEM images show that the morphology of the samples is different after the addition of maleic acid or urea in synthesis precursor. For crystals synthesized in the presence of urea, they seem to be agglomerates of plate like crystallites with fine and defined shapes. In the case of maleic acid, crystals are also agglomerates of crystals, bigger than the urea samples, but with very thin layered crystallites. The SEM images also show that the sample obtained from higher amount of addition of maleic acid has batter shapes.

Although the morphology of the samples with urea or maleic acid is quite different, EDS analysis revealed a V/P ratio with close values, being about 0.7 for both samples VPO_7 and VPO_4.

The acidic and basic character of the additives may be responsible for this difference, since chemical environment can influence the oxidation state of vanadium samples. It has been reported previously that crystallization under mildly reducing conditions in aqueous solutions yielded compounds containing reduced vanadium clusters [31], and that under weakly acid or basic conditions vanadium coordination polyhedra can polymerize into finite clusters and at low pH, chains and sheets of polyhedra can be formed.

### 3.2.2 Influence of synthesis time

As this is a systematic study on how the synthesis conditions influence the formation of vanadium phosphate phase, time is one of the studied parameters. It is known that synthesis time is one of the most important parameters in hydrothermal synthesis, since every crystal phase has a typical induction period (the amount of time between the beginning of the reaction and the beginning of the crystallization process). Also, these experiments are useful to explore if any other structural and/or chemical intermediates are formed during synthesis period.

Since the crystallinity of the samples synthesized with the addition of maleic acid is very low, the influence of synthesis time on the formation and crystallinity of this product was studied. Composition of sample VPO_7 was used for this experiment. Normally, the sample was synthesized for 7 days at 170 ºC. In this experiment, samples were synthesized at 170 ºC for periods of 5, 10 hours, 1-7 days, 2 and 3 weeks. XRD results are presented in Figures 3.22, 3.23 and 3.24.

XRD patterns of the initial phases of crystallization (Figure 2.22) indicate a dynamic process, since the XRD of samples of 5 and 10 hours synthesis are very distinct, revealing the formation of different products in a short period of time. The patterns of samples synthesized in the range of 1 to 7 days are very similar, revealing that there are not many alterations in the product. The important phase transformation occurs in one day, since between the periods of 1 to 7 days, the formed phase is stable, indicating that for the synthesis of this phase reaction times can be reduced.

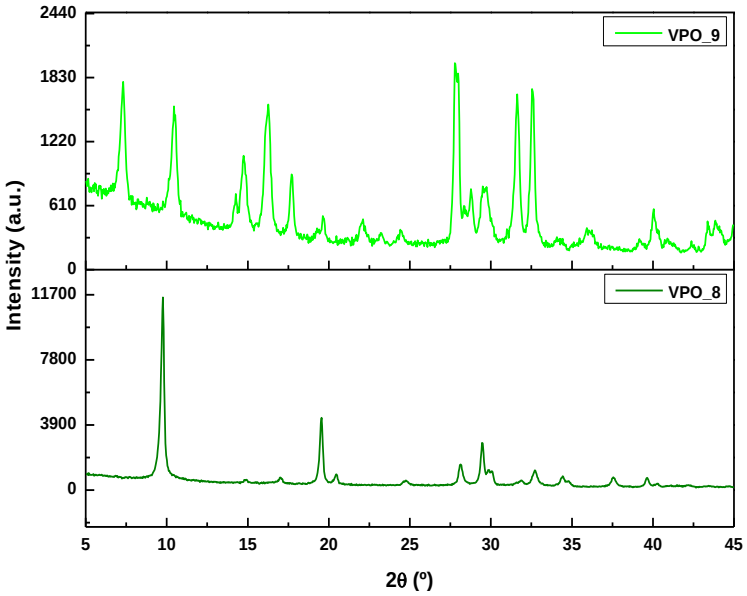


**Figure 3.22-** XRD patterns of samples VPO_8 and VPO_9, for synthesis periods of 5 and 10 hours, respectively.

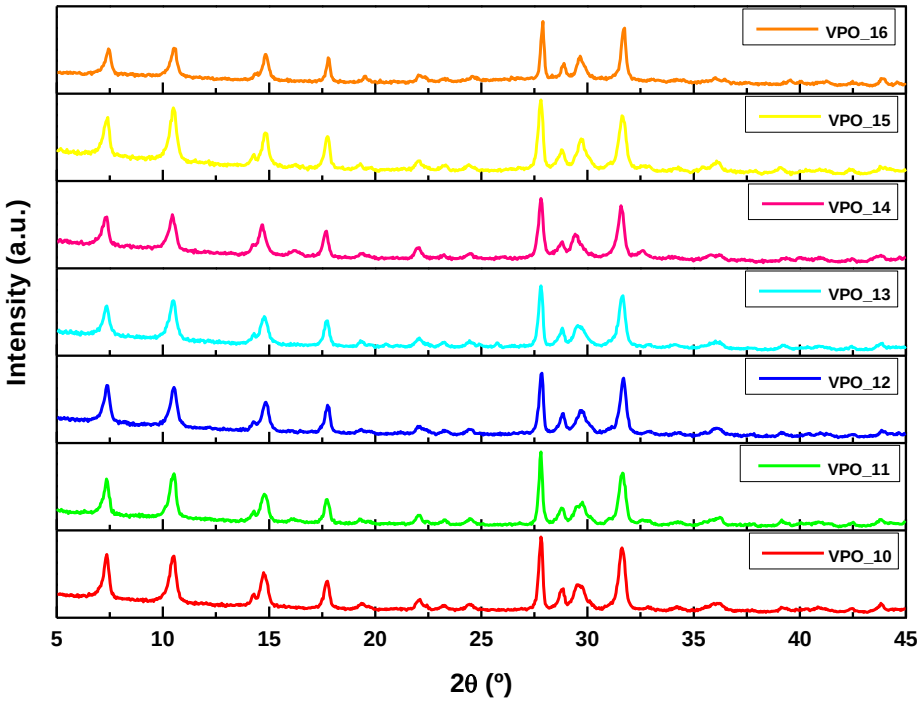


**Figure 3.23-** XRD patterns of samples VPO_10-16, for different synthesis periods.

For longer periods of synthesis, another crystalline phase formed, the XRD pattern of which is presented in Figure 3.24. The formed product is stable for periods of 2 and 3 weeks although the sample of 2 weeks' seems better than other. The further study indicated that it may have the structure very similar to $Na_3V_2O_2(PO_4)_2F$.

Concerning the morphology of the samples (Figure 3.25), VPO_8 and VPO_9 show apparent differences, which are in agreement with the XRD data. Comparing SEM images of VPO_9 and VPO_10, besides the size of the crystal agglomerates, the morphology of the samples are very similar.

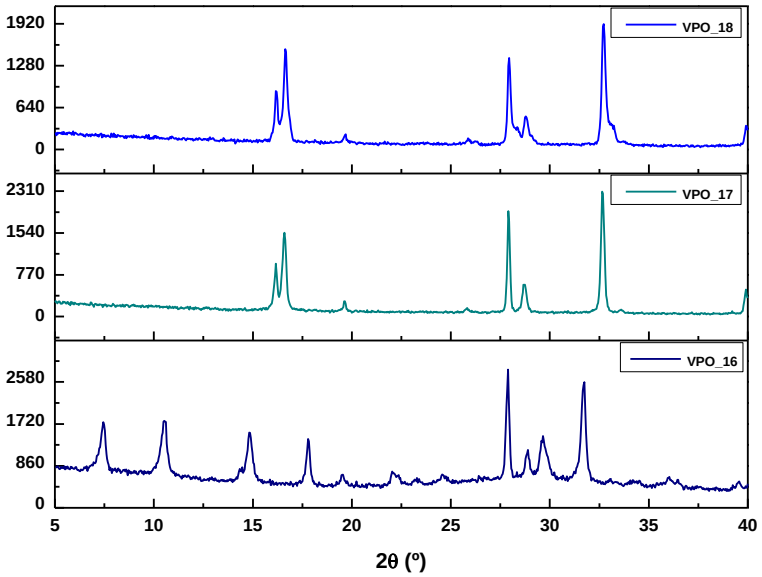


**Figure 3.24-** XRD patterns of samples VPO_16-18, that correspond to synthesis periods of 1, 2 and 3 weeks.

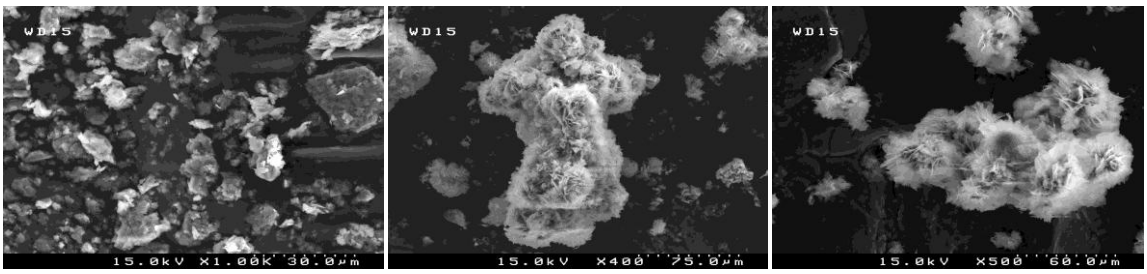


**VPO_8** **VPO_9** **VPO_10**

**Figure 3.25-** SEM images for samples VPO_8, VPO_9 and VPO_10, respectively.

### 3.2.3. Influence of the solvent

It is nowadays common in microporous materials synthesis, to substitute water by different solvents like organic solvents, ion liquids, etc, so that the amount of water in the starting mixture can be controlled as a reagent. In order to

study the influence of solvent on the previously obtained vanadium phosphate phase [23], synthesis with different solvents were attempted.

One of the solvents used was ethylene glycol (Figure 3.26). The use of glycol solvents in place of water is not a completely new route (this type of process is even referred as glycothermal reaction), or even in the synthesis of vanadium (III) phosphate phases. Nakamura *et al.* [32] reported the synthesis of two phases that depend on factors like P/V ratio, vanadium source, temperature and solvent, where 1,4-butanediol was used.

In the present work, the organic solvent chosen was ethylene glycol, also named 1,2-ethanediol, replacing part of the water and maintaining the same V/P ratio. Samples with 25 and 50 wt% of ethylene glycol (replacing wt% of water) were synthesized and correspond to samples VPO_19 and VPO_20 respectively. XRD results are presented in Figure 3.27.

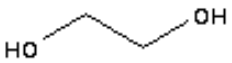


**Figure 3.26-** Ethylene glycol structure, $C_2H_6O_2$ [33].

XRD results of these two samples are very different, indicating that different phases were formed. It is interesting to notice that the peak position in XRD pattern of the sample synthesized with 25 % of ethylene glycol is very close to the XRD pattern of samples synthesized with maleic acid (VPO_7), although the intensities are different, which can reveal structure similarity. These two different organic additives contain hydroxyl groups, that may play an important role in the synthesis and in the formation of this phase. So, ethylene glycol, acted not only as solvent (together with $H_2O$) and can induce different phase formation. It is also important to notice that only with relative high amount of water in the precursor solution, the phase was obtained, showing that water also has an important role in

the formation of this product. In fact, an experiment with only ethylene glycol was carried out, but it didn´t produce a powder product that could be analyzed.

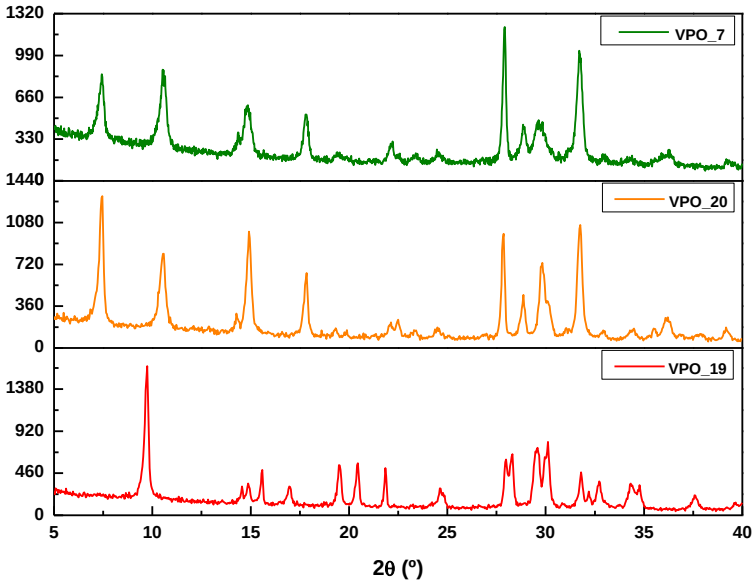


**Figure 3.27-** XRD patterns of samples VPO_7, VPO_19 and VPO_20.

Another different type of solvent used in this work was the eutectic mixture. As it was previously mentioned, eutectic mixtures have mimic ionic liquids' properties and are very interesting alternative solvents in the synthesis of microporous materials. The eutectic mixture used in this work, is constituted by choline chloride and urea (detailed description of its composition and preparation can be found in chapter 2).

Synthesis without water and with eutectic mixture as only solvent generate low crystalline product with few peaks at high 2θ in the XRD presented in Figure 3.28. The product clearly contains amorphous materials.

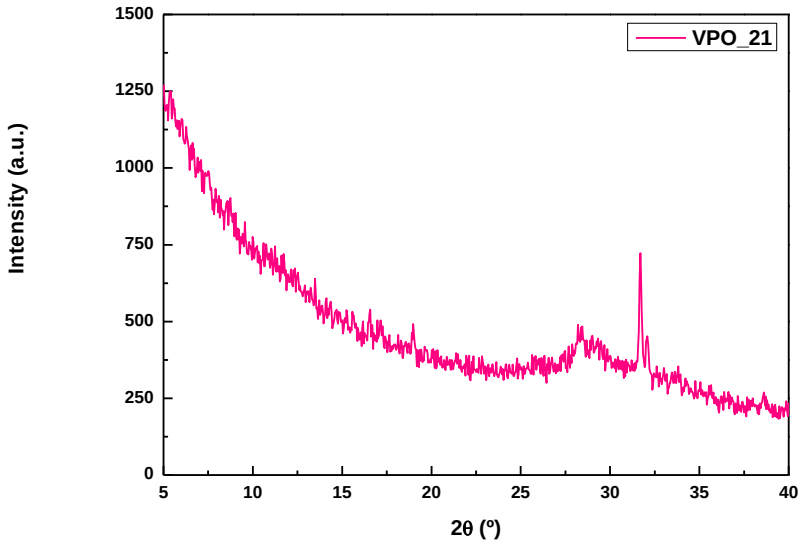


**Figure 3.28-** XRD result of vanadium phosphate sample synthesized with eutectic mixture used as a solvent (sample VPO_21).

Since the previous experiment produced sample with very low crystallinity, different amounts of water were also added in order to ensure complete dissolution of vanadium and phosphorous sources, to explore if water is essential for the formation of crystalline products in this system. Molar compositions are listed in Table 2.2 (chapter 2). XRD results are shown in Figure 3.29.

The addition of small amounts of water, together with the presence of eutectic mixture, results in the formation of a crystalline phase. The XRD for all three samples is the very similar. For the sample with the least amount of water the first peak is not intense, but the peak position is the same. The XRD search-match points out that this is a known phase, trisodium oxovanadium phosphate(V) hydrogenphosphate $Na_3VO(PO_4)(HPO_4)$, a layered structure that exhibits vanadium in valence (IV), with the $VOPO_4$ layer as a fundamental building unit [34].

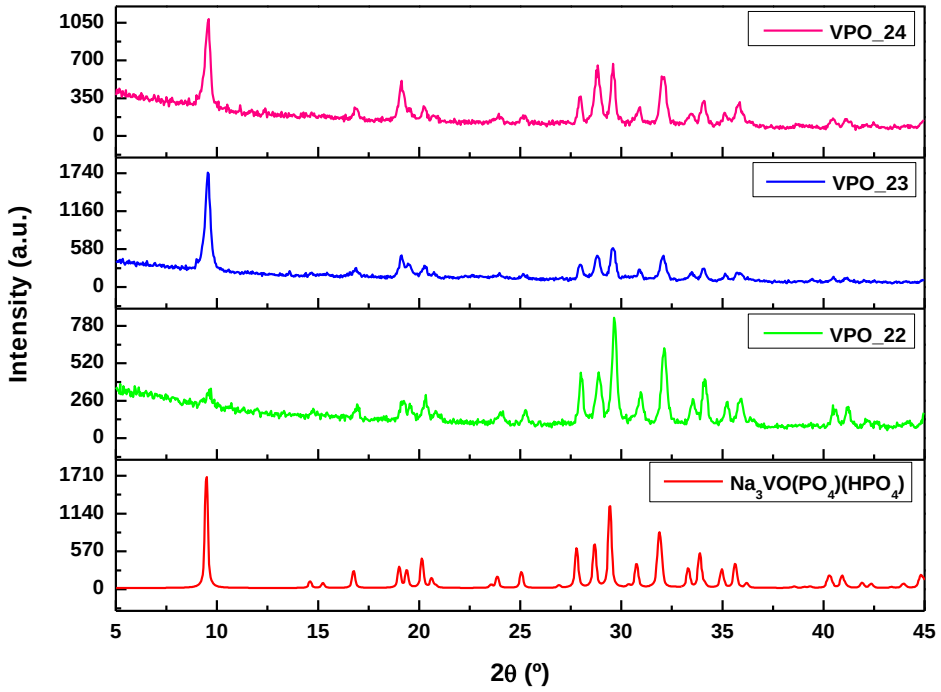


**Figure 3.29-** XRD results of samples VPO_22, VPO_23 and VPO_24 and the calculated XRD pattern of $Na_3VO(PO_4)(HPO_4)$.

The resulting powder is pure, no other crystalline phases were identified from the powder XRD matching. The differences in peak intensity among the three XRD diffractograms can also be related to the fact that this is a layered structure. In a study on several vanadium phosphates, where the $NH_4$ /V/P/$H_2O$ system was referred, the authors reported the formation of the same phase, $Na_3VO(PO_4)(HPO_4)$ and they study the influence of several different parameters on the $NH_4$ /V/P/$H_2O$ system (pH, organic cations presence, Na/V ratio, $Na^+$ concentration, vanadium source and its oxidation state), and this phase is obtained only under specific synthesis conditions [34]. Here we obtained the same product by carrying out the synthesis hydrothermally using water and eutectic mixture ChCl:urea.

Furthermore, results for samples previously synthesized with the addition of urea and samples synthesized with water and eutectic mixture are similar (Figure

3.30). The XRD patterns are very close, and most of the peaks are at same positions.

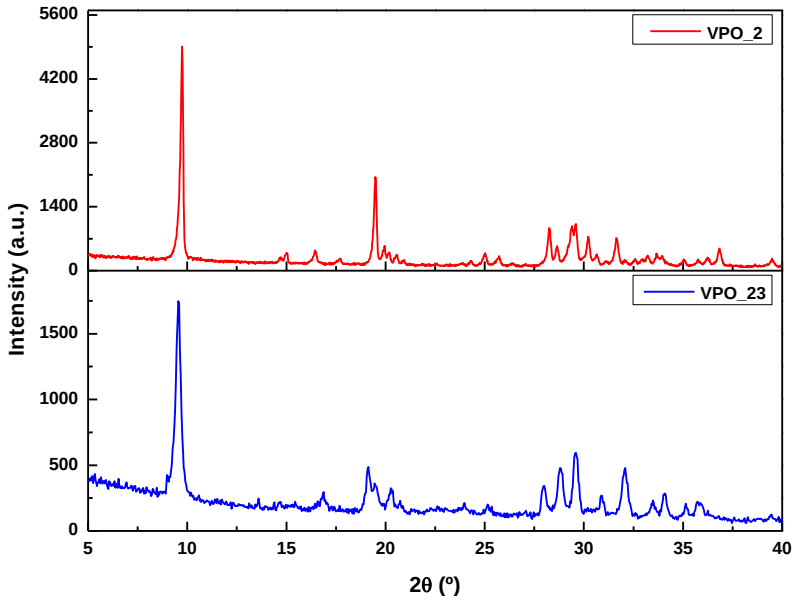


**Figure 3.30-** XRD results of samples VPO_4 and VPO_23.

Although to fully understand the role of organic additives in the synthesis of crystalline products in our system (general composition 1.0 $VO_2$- 4.4 $P_2O_5$- 4.4 $Na_2O$ – 247.61 $H_2O$) requires more experiment, the previous results suggest that water amount definitely plays an important role on the synthesis. Samples where the amount of water decreased cannot produce well crystallized products, examples are seen in the case of substitution of solvent by ethylene glycol and eutectic mixture ChCl:urea. It is also important to note that, closely related with the amount of water present in precursor solutions, is the pH value; another parameter whose influence need be further studied.

Of course many other parameters can influence the synthesis, but results here indicate that the amount of water present in the initial solution/gel may be a key point for synthesis in the studied system.

### 3.2.4 Influence of the heating process

Microwave heating assisted synthesis, as an alternative method to conventional heating, was also applied to the vanadium phosphate system. Although much of the reported synthesis of microporous materials refer to hydrothermal method, microwave assisted synthesis may present some advantages, mainly by reducing the time of the synthesis. For this experiment, samples with VPO_7 composition (Table 2.2) were synthesized for periods of 1 and 5 hours. The resulting XRD patterns are presented in Figure 3.31.

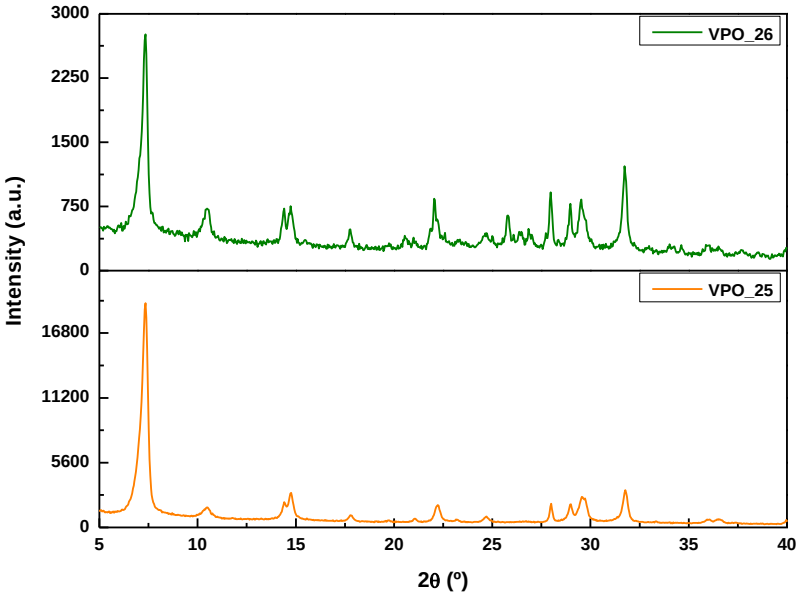


**Figure 3.31-** XRD results of vanadium phosphate samples VPO_25 and VPO_26.

XRD patterns are very similar for both samples, presenting the same symmetry but different relative intensities. It is curious to notice that with only one hour of microwave synthesis, crystallinity is higher than for a longer period of synthesis, indicating that 1 hour is enough for the synthesis of this phase (under these conditions of microwave heating). Although the molar composition of the starting mixture is the same as VPO_7, XRD results seem quite different. XRD search-match suggests the existence of $Na_3VP_8O_{23}$ and $V_4O_7$ in sample VPO_25. However, careful comparison of detailed XRD pattern does not confirm this

identification. Close inspection of the powder XRD patterns of samples VPO_25 and VPO_7 indicates that both present reflection peaks at very similar 2θ although the intensities are very different. The first XRD peak of sample VPO_25 is much stronger than others.

SEM pictures are depicted in Figures 3.32 and 3.33.

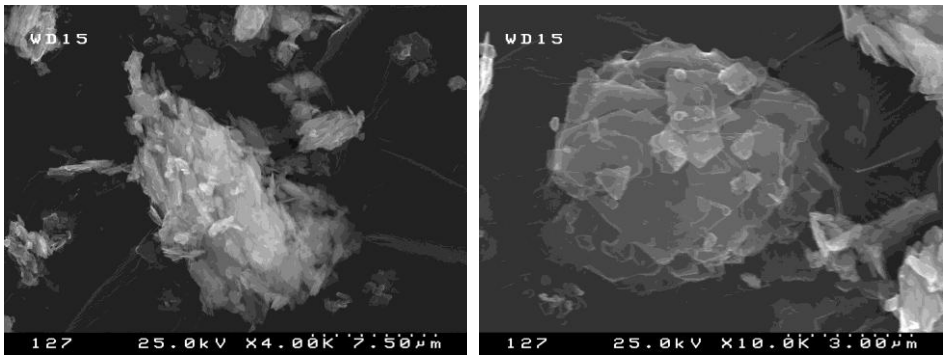


**Figure 3.32-** SEM images of sample VPO_25.

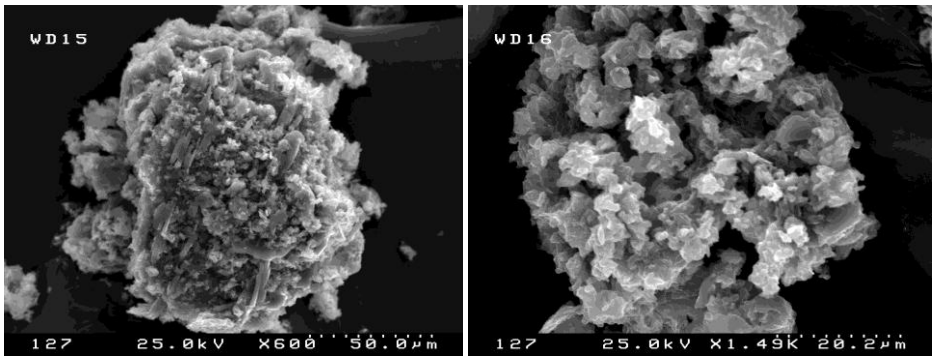


**Figure 3.33-** SEM images of sample VPO_26.

SEM images of these samples, presented in Figure 3.32 and 3.33, and show that with a longer period of microwave heating, the sample is less crystalline than the one heated for only 1 hour (that has more defined shapes and less amorphous part). Morphology of the sample VPO_25 is similar to the samples synthesised with the same composition and through the conventional heating.

It is interesting to observe that, with the same composition and synthesis time (5 hours), the different heating processes, microwave (VPO_26) and

conventional heating (sample VPO_8), resulted in different final products. This can be attributed to the much efficiency of microwave heating.

### 3.2.5 Formation of known crystalline phases

It has been mentioned before that vanadium phosphate syntheses under different experimental conditions resulted in some known crystalline phases, identified through XRD matching process. Some details have been studied and presented as follows.

#### 3.2.5.1 Sodium vanadyl (IV) orthophosphate, Na(VO)($PO_4$)

Synthesis of vanadium phosphate without any additives resulted in a known phase matched by XRD analysis, sodium vanadyl (IV) orthophosphate, Na(VO)(PO4). XRD peaks of the as-synthesized sample VPO_1 match almost all peaks of Na(VO)($PO_4$) pattern (Figure 3.15).

The structure of Na(VO)($PO_4$) is depicted in Figure 3.34. It is composed of infinite chains of trans-corner-sharing [$VO_6$] octahedra along *c* direction (Figure 3.34a) [35]. Parallel chains are maintained together through corner-sharing 4 oxygen atoms with [$PO_4$] tetrahedral (Figure 3.34b, c), forming a zig-zag like arrangement. The resulting voids of this framework are filled with Na atoms. Along c direction, the connection of the [$PO_4$] tetrahedra to the trans-corner-sharing infinite chains of [$VO_6$] octahedra can be seen better. Each [$PO_4$] tetrahedron is linked to 4 [$VO_6$] octahedra in 3 different [$VO_6$] octahedral chains. One [$VO_6$] chain shares two octahedra with a same [$PO_4$] tetrahedron while the other two [$VO_6$] chains share only one (Figure 3.34c).

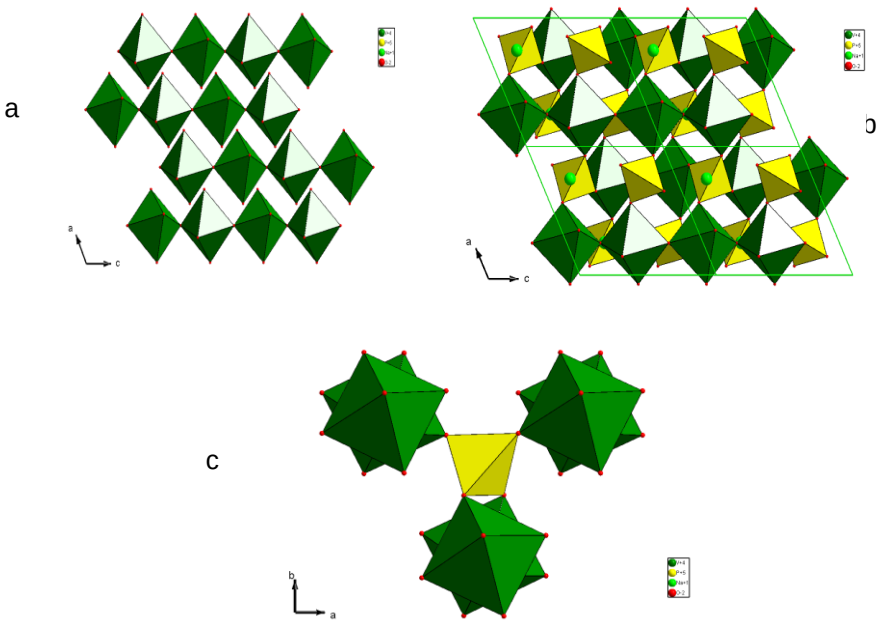


**Figure 3.34-** Polyhedral representation of Na(VO)(PO4) structure, (a) trans-corner-sharing [$VO_6$] octahedral chains, (b) structure view along *b* direction and (c) the connection of [$VO_6$] and [$PO_4$] .

FTIR spectra of sample VPO_1 was recorded for further confirmation of the structure, and is presented in Figure 3.35. Peaks at ca. 1020 and 1150 $cm^{-1}$ can be attributed to symmetric stretching of the $PO_4$ tetrahedra units, while band at ca. 670 $cm^{-1}$ can be due to vibrations of O-P-O groups [36]. Bands in the range of 500-700 $cm^{-1}$ are attributed to V-O-V linkages bending and stretching modes. In some works that report structures having $V^{IV}$=O groups [37], FTIR spectra shows a band at 960 $cm^{-1}$ attributed to the presence of that group. A small band is noticed around this wavelength in FTIR spectrum of our sample although in the structure of Na(VO)($PO_4$) does not exist $V^{IV}$=O group. However, this is reasonable because in this structure the bond length of $VO_6$ is between 1.643 and 2.111 Å.

DR UV-Vis spectrum for this sample was also recorded (Figure 3.35), to obtain more information on the structure the oxidation state of vanadium. Absorption bands around 250 nm are known to be due to CT transitions between $O^{2-} \rightarrow V^{4+}$ type, as well as the presence of broad bands between 550-650 nm [36]. The spectrum in Figure 3.36 shows an intense band at ca. 260 nm and another weaker band at ca. 650 nm, that can be due to the presence of vanadium species

with valence IV, confirming its presence in this sample. Furthermore, the colour of this sample is pale green, which is responsible for the weaker and broad absorption band between 450 and 550 nm [1] due to $V^{4+}$ d–d transition.

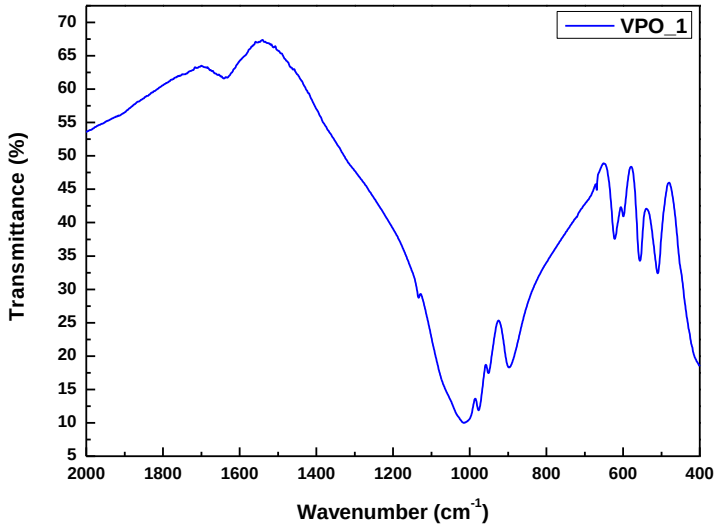


**Figure 3.35-** FTIR spectrum of sample VPO_1.

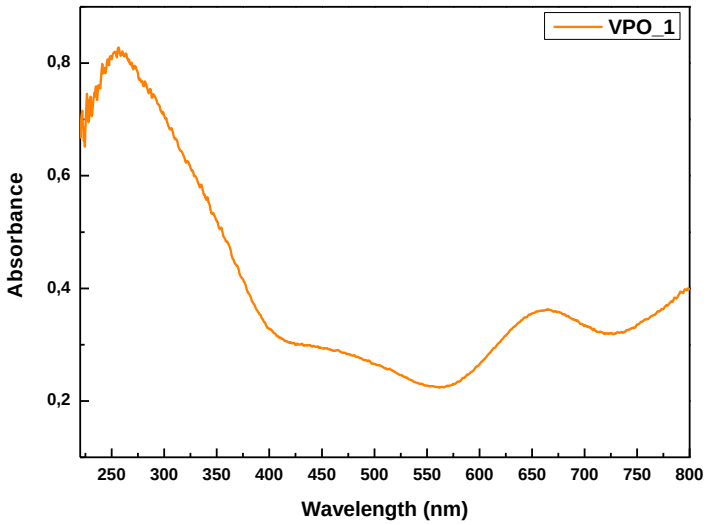


**Figure 3.36-** DR UV-Vis spectrum of sample VPO_1.

### 3.2.5.2 Sodium vanadium fluorophosphates $Na_3V_2O_2(PO_4)_2F$ and $Na_3V_2(PO_4)_2F_3$

For as-synthesized samples VPO_17 and VPO_18, XRD analysis suggested a crystalline phase $Na_3V_2O_2(PO_4)_2F$. The structure similarity can be seen from XRD results in Figure 3.37. XRD of sample VPO_18 shows some extra peaks at ca. 28 and 33º 2θ, indicating that sample VPO_17 is purer than VPO_18 and better fits the XRD pattern of the sodium vanadyl (IV) fluoride phosphate phase. In Figure 3.37 another structurally related phase, $Na_3V_2(PO_4)_2F_3$, is also presented for comparison.

The XRD patterns of those two sodium vanadium fluorophosphates phases are very similar. The most notable difference is that the XRD of $Na_3V_2(PO_4)_2F_3$ shows extra peaks at ca. 12.8, 23.5 and 30.8º 2θ region. This strongly suggests that in samples VPO_17 and VPO_18 the present phase is $Na_3V_2O_2(PO_4)F$.

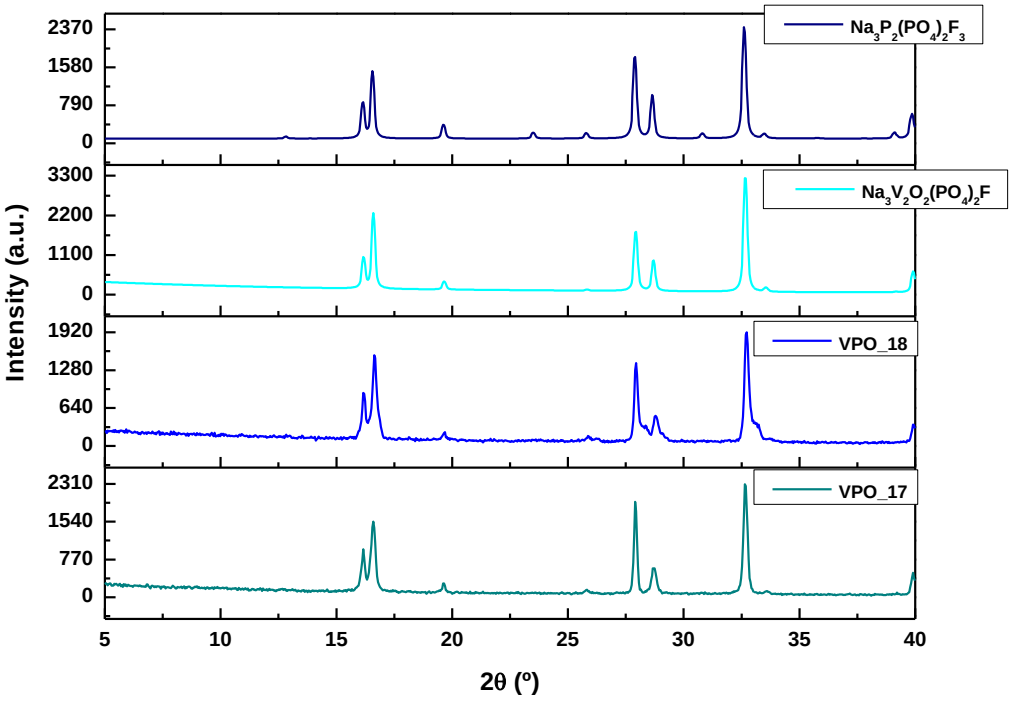


**Figure 3.37-** XRD of samples VPO_17 and VPO_18, and calculated XRD pattern of $Na_3V_2O_2(PO_4)_2F$ and $Na_3V_2(PO_4)_2F_3$ phases.

$Na_3V_2O_2(PO_4)_2F$ belongs to a family of materials with the structure of the mineral natisite, that shows rich chemistry and exhibits good insertion/de-insertion properties, and have important applications as cathode materials for batteries. The crystalline structure of $Na_3V_2O_2(PO_4)_2F$ is composed of layers of intercalated [$VO_5F$] octahedra and [$PO_4$] tetrahedra by sharing O vertices parallel to the *ab* plane. Along *c* direction [$VO_5F$] octahedra are connected per pair via F vertices located in the same plane (*ab*) as the disordered Na atoms [38].This structure is depicted in Figure 3.38. $Na_3V_2O_2(PO_4)_2F$ was synthesized hydrothermally in NaF-$VO_2$-$Na_3PO_4$-CuO-$H_2O$ system at 280 ºC with a pressure of 100 bar for 20 days [39]. The distribution of $Na^+$ cations in small pore depends on the synthesis condition [38, 39].

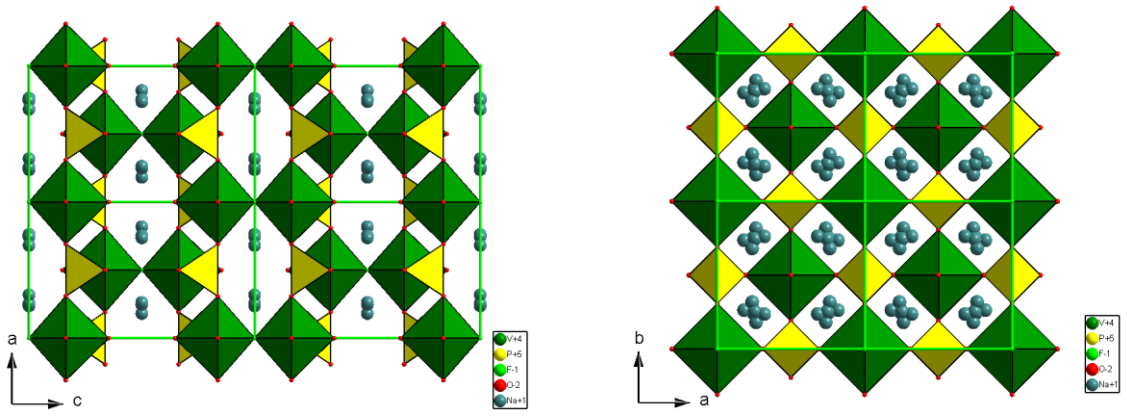


**Figure 3.38-** Polyhedral representation of $Na_3V_2O_2(PO_4)_2F$, along *b* direction (left) and along *c* direction (right).

Another, structurally related material initially identified in the XRD report, is $Na_3V_2(PO_4)_2F_3$. It also has applications as cathode material for batteries, although it shows lower electronic conductivity [40]. As it can be observed in the polyhedral representation of $Na_3V_2(PO_4)_2F_3$ structure (Figure 3.39), this crystalline structure is characterized by an extended three-dimensional framework, built up from [$V_2O_8F_3$]

bi-octahedral and [$PO_4$] tetrahedral units. The [$V_2O_8F_3$] bi-octahedral units are bridged by one fluorine atom, while the sodium ions are distributed in the resultant network [40]. The oxygen atoms are all interconnected through the [$PO_4$] units. This arrangement results in the formation of channels along *a* and *b* directions [41]. According to literature, for the synthesis of the powder sample of this material, a specific route was followed [42]. First, a $V_2O_5$ powder dissolved in phosphoric acid ($H_3PO_4$), is reduced by $N_2H_4$ – $H_2O$ solution. Then NaF is added in a molar ratio of 4.3Na/2V. The whole mixture is introduced in a Teflon lined stainless steel autoclave and heated at 180 ºC during 64 Hours (about 2.5 days) [42].

One of the main differences between these two sodium vanadium fluorophosphate phases is the oxidation state of vanadium; in $Na_3V_2O_2(PO_4)_2F$ the phase presents V(IV), and in $Na_3V_2(PO_4)_2F_3$ one presents V(III).

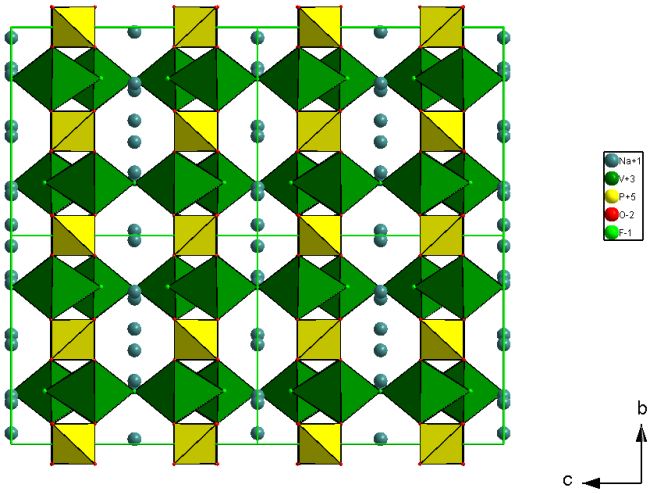


**Figure 3.39-** Structural representation of $Na_3V_2(PO_4)_2F_3$, along *a* direction.

The results of sample VPO_17 and VPO_18 are interesting due to following reasons: the sample was prepared hydrothermally at lower temperature and for shorter time than in $Na_3V_2O_2(PO_4)_2F$ synthesis; the similar XRD pattern to a fluoride containing vanadium phosphate strongly suggests the structure similarity. From the structure of point view, a material with this structure and without fluoride is possible. The F-V bond length in $Na_3V_2O_2(PO_4)_2F$ is 2.108 Å while the O-V bond

length of the opposite corner is 1.625 Å. It is not surprise that O replace F to connect two [$VO_6$] octahedra and with $H^+$ nearby to compensate the extra charge. With this in mind, we re-search XRD database, however, no such kind of material exists. This material is subject to further study.

DR UV-Vis spectra of samples VPO_17 and VPO_18 are presented in Figure 3.40. Spectrum of sample VPO_17 presents defined bands at ca. 250 nm, 350 nm and a broader band at ca. 660 nm. A small shoulder in the 450 nm region can also be noticed. According to literature [43], d-d transitions of V(IV) result in bands at 420-450 and 650 nm, and show the green color of the final product. In VPO_18, the separation between the maximum at ca. 250 nm and 350 nm is not so clear seen, but it can be identified. This can possibly be due to overlay of CT bands. The presence of bands related to the presence of V(IV) suggests that the phase present in these samples is closer to $Na_3V_2O_2(PO_4)_2F$ (vanadium oxidation state IV).

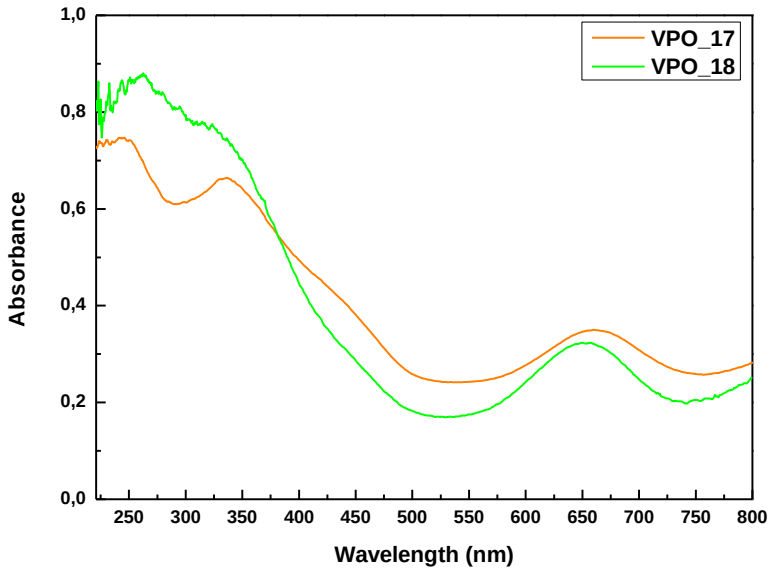


**Figure 3.40-** DR UV-Vis spectra of samples VPO_17 and VPO_18.

In order to further investigate the similarity between the synthesized samples and the $Na_3V_2O_2(PO_4)_2F$ phase, and because no fluorine was added to the synthesis mixture EDS analysis was performed. SEM pictures were also recorded for morphological elucidation. These results are presented in Figures 3.41, 3.42 and 3.43 and in Table 3.3.

In fact, both samples do show the presence of fluorine although it cannot be quantified. The reason is not clear now. But this can be the result of contaminations that may have occurred during the experimental preparation of the precursor solution (contamination in the mixing cup, contamination in the Teflon itself or, most unlikely, contamination in the reagents). Studies for these samples and synthesis conditions are continuing in order to explain these results.

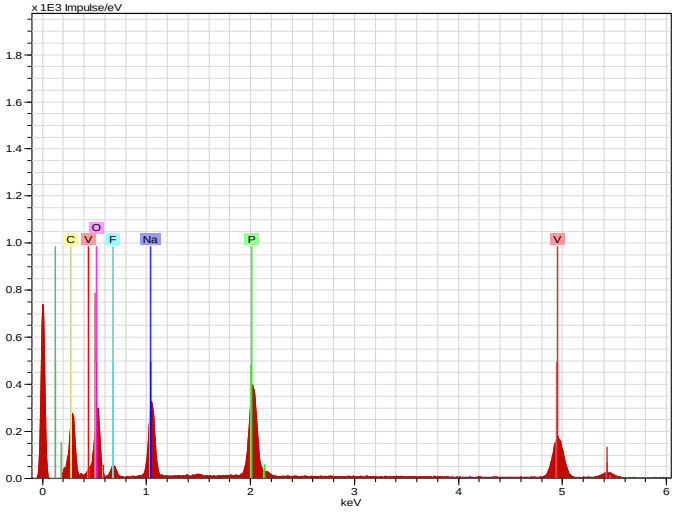


**Figure 3.41-** EDS result for sample VPO_17.

**Table 3.3 -** EDS results and relative element ratios for samples VPO_17 and VPO_18.

| | V/P | V/Na |
|---|---|---|
| VPO_17 | 1.18 | 0.827 |
| VPO_18 | 1.01 | 0.756 |

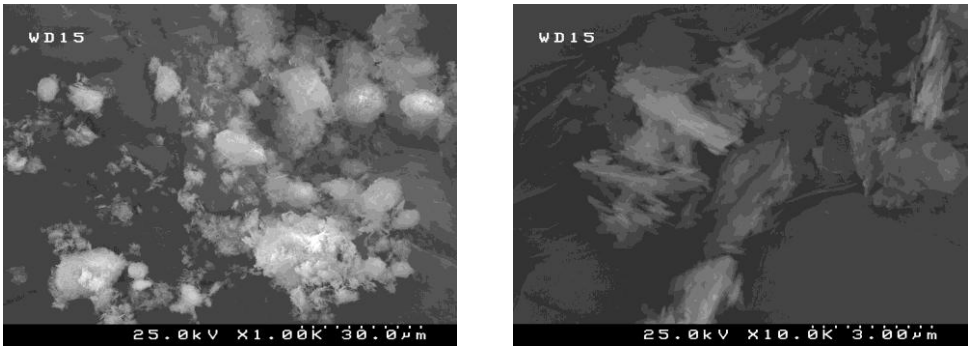


**Figure 3.42-** SEM images of sample VPO_17.

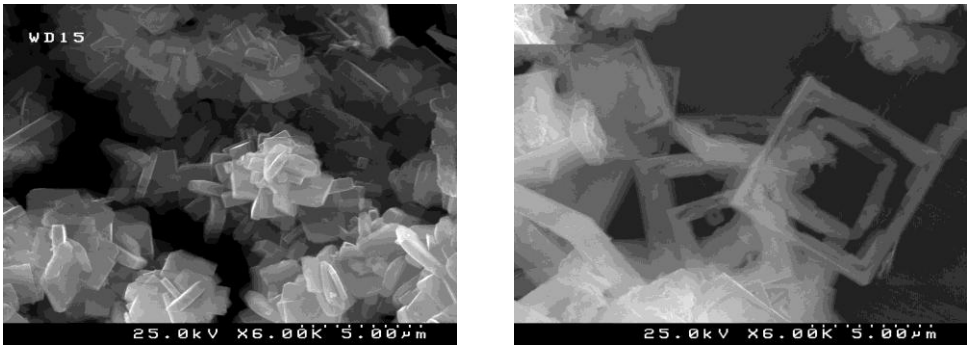


**Figure 3.43-** SEM images of sample VPO_18.

Morphologically, samples VPO_17 and VPO_18 seem to be very distinct. In sample VPO_17, crystals are very small and fine, and are present in agglomerates of smaller crystals that have no regular shape. For sample VPO_18, crystals are well defined, seem to be a little bigger than the previous ones and present a particular hollow square shape. Although XRD patterns of these two samples are very similar, morphology is distinct. This can be due to longer time of synthesis.

FTIR spectrum of sample VPO_17 (Figure 3.44) was also recorded for more detailed structural description. Several characteristic peaks of V-O vibrations exist in lower wavenumber region (500-1000 $cm^{-1}$). Peaks at ca. 555 and 680 $cm^{-1}$ are attributed to the vibration of the V-O nbonds and the sharp peak at ca. 921 $cm^{-1}$ to the vibration of V=O bonds, which is the typical peak for the vanadyl short bond. In higher wavenumber region, peaks at ca. 1040, 1150 are vibrations attributed to $(PO_4)^{3-}$ tetrahedral unit. This spectrum is very similar to the one

reported to $Na_{1.5}VOPO_4F_{0.5}$ [38], which proves that the chemical environment of framework atoms in sample VPO_17 is very similar to the one in sodium vanadyl(IV) fluorophosphate.

This type of vanadium phosphates is important and used as cathode materials for batteries. In this context, an easier and short time process of production of this type of material is very useful. The synthesis of $Na_3V_2O_2(PO_4)_2F$ may be further optimized by the small modification of this process.

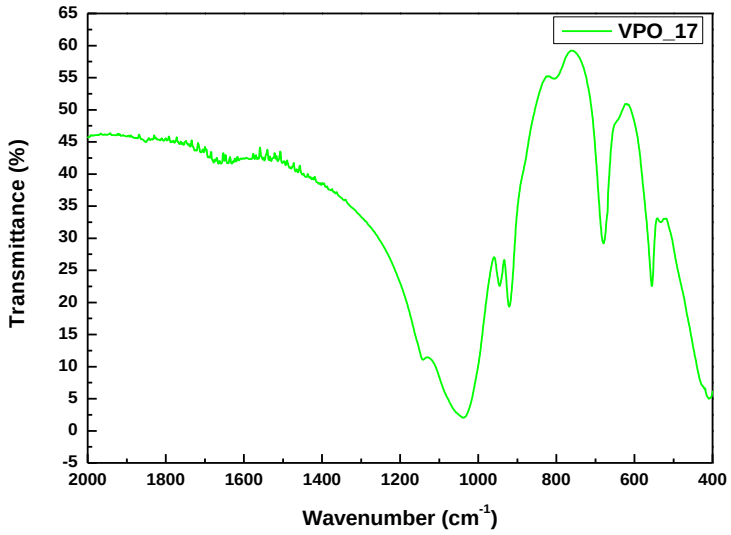


**Figure 3.44-** FTIR spectrum of sample VPO_17.

### 3.2.5.3 Trisodium oxovanadium phosphate (IV) hydrogenophosphate, $Na_3VO(PO_4)(HPO_4)$

Samples synthesized with eutectic mixture ChCl:urea and in the presence of water resulted in the crystalline phase $Na_3VO(PO_4)(HPO_4)$. Polyhedral representations of the structure are presented in Figure 3.41. The structure of this material is similar to many previously reported layered vanadium phosphates, having $VOPO_4$ layer as the fundamental building unit (Figure 3.41a) [34]. The layers

are formed by $VO_6$ octahedra connected through four oxygen atoms of the planar around V to four $PO_4$ tetrahedra. Also, the $VO_6$ octahedron is connected to $HPO_4$ group via corner sharing (Figure 3.46b) at layer surface.

According to the work of Schindler *et al.* [34], this phase can be synthesized under different conditions, for example in the system $V_2O_5/H_3PO_4/NaOH/H_2O$ with a molar ratio of 1/8/14/1440, under pH 6.5, at 200 ºC for 10 days; and also in the system $VOSO_4/H_3PO_4/NaOH/H_2O$ with the respective molar ratios of 1/4/7/700 at pH 6.4 for 12 days, or 1/4/8/700 at pH 6.9 for 12 days.

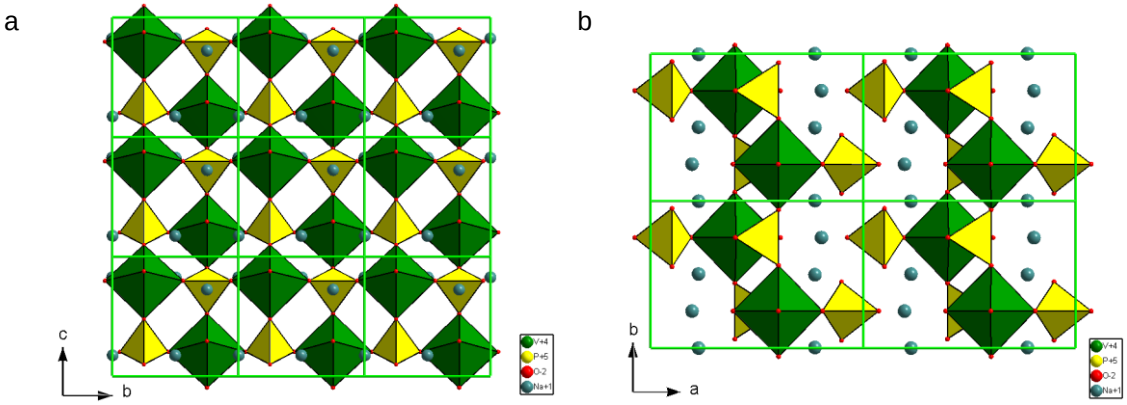


**Figure 3.45-** Polyhedral representations of $Na_3VO(PO_4)(HPO_4)$, along *a* direction (left) and along *c* direction (right).

The synthesis conditions used in this work are different from published ones, being at slightly lower temperature (170 ºC) and for a shorter period (7 days), and using different molar composition and different P source. The synthetic procedure for this phase may be further optimized. Previously in this chapter, it was showed that the product of this synthesis must depend on the amount of water in the initial gel, which is intimately related with pH of the solution. Although in this work, pH is not a variable carefully controlled, it can clearly influence the crystallization process. Urea species (and derivative ammonia products of urea decomposition) may also play a role in this synthesis, and further studies on these influences may be carried out in future.

These exemplify once again the large variability of the vanadium phosphate system and the different response to the variation of various synthesis parameters.

## 3.3 References

[1] S. Ferdov, Z. Lin, R.A.S. Ferreira, M.R. Correia, *Micropor. Mesopor. Mater.* 110 (2008) 436.

[2] R. Szostak, *Molecular Sieves*, Van Nostrand Reinhold, new York (1989) 205.

[3] X. Wang, L. Liu, L. Wang, A.J. Jacobson, *Mater. Res. Soc. Symp. Proc.* 848 (2005) F.F. 3.2.1.

[4] L. Ctanzaro, P. De Luca, J.B. Nagy, A. Nastro, in: E.W.J. van Steen, L.H. Callanan, M. Claeys and C.T. O'Connor (Eds.), Proceedings 14th Interntional Zeolite Conference (2004) 746.

[5] J. Perez-Ramirez, F. Kapteijn, G. Mul, X. Xu, J.A. Moulijn, *Catal. Today* 76 (2002) 55.

[6] A.Z. Ma, W. Grünert, *Chem. Commun.* (1999) 147.

[7] G.D. Pirngruber, P.K. Roy, R. Prins, *J. Catal.* 246 (2007)147.

[8] F.Q. Chen, M.H.Do, W. Zheng, D.G. Cheng, X.L. Zhan, *Catal. Commun.* 9 (2008) 2481.

[9] L.V. Pirotko, V.S. Chernyavsky, A.K. Uriarte, G.I. Panov, *Appl. Catal. A* 227 (2002) 143.

[10] N. Shiju, S. Fiddy, O. Sonntang, M. Stockenhubrec, G. Sankor, *Chem. Commun.* (2006) 4955.

[11] C. Li, *J. Catal.* 216 (2003) 203.

[12] C. Wu., Y. Kong, F. Gao, Y. Wu, Y. lu, l. Dong, *Micropor. Mesopor. Mater.* 13 (2008) 163.

[13] M. Schwidder, M.S. Kumar, U. Bentrup, J. Pérez-Ramirez, A. Brückner, W. Grünert, *Micopor. Mesopor. Mater.* 111 (2008) 124.

[14] T. Abe, Y. Tachibana, T. Uematso, M. Iwamoto, *J. Chem. Soc., Chem. Commun.* (1995) 1617.

[15] P. Selvama, S.E. Dapurkar, S.K. Badamali, M. Murugasan, H. Kuwano, *Catal. Today* 68 (2001) 69.

[16] M.S. Kumar, M. Schwidder, W. Grünert, A. Brückner, *J. Catal.* 227 (2004) 69.

[17] B. Echchahed, A. Moen, D. Nicholson, L. Bonneviot, *Chem. Mater.* 9 (1997) 1716.

[18] A. Tuel, I. Arconb, J.M.M. Milleta, *J.Chem. Soc., Faraday Trans.* 94 (1998) 3501.

[19] N.A. Turta, M. Veltri, D. Vuono, P.De Luca, A. Nastro, *J. Porous Mater.* 16 (2008) 527.

[20] T. Amaroli, G. Busca, F. Miella, G.P. Toledo, A. Nastro, P. De Luca, G. Bagnasco, M. Turco, *J. Mater. Chem.* 10 (2000) 1699.

[21] A. Philippou, M.W. Anderson, *Zeolites* 16 (1996) 98.

[22] M. Naderi, M.W. N. Aderson, *Zeolites* 17 (1996) 437.

[23] S. Ferdov, M.S. Reis, Z. Lin, R.A.S: Ferreira, *Inorg. Chem.* 47 (2008) 10062.

[24] G. Ladwig, K.H. Jost, K. Schlesinger, *Z. Chem.* 19 (1997) 386.

[25] B. Tofield, G.R. Crane, G.Pastuer, R. Sherwood, *J. Chem. Soc. Dalton Trans.* (1975) 1806.

[26] J.T. Vaughey, W.T.A. Harrison, A.J. Jacobson, D.P. Goshern, J.W. Johnson, *Inorg. Chem.* 33 (1994) 2481.

[27] M. Schindler, W. Joswig, W.H. Baur, *Eur. J. Solid State Inorg. Chem.* 32 (1995) 109.

[28] A. El Badraoui, J.Y. Pivan, M. Maunaya, M. Louër, D. Louër, *J.Alloys Comp.* 245 (1996) 47.

[29] http://webbook.nist.gov/cgi/cbook.cgi?Name=maleic+acid&Units=SI

[30] http://webbook.nist.gov/cgi/cbook.cgi?Name=urea&Units=SI

[31] A. Müller, J. Döring, *Z. Anorg. Allg. Chem.* 595 (1991) 251.

[32] T. Nakamura, T. Inui, M. Inoue, T. Miyake, *J. Mater. Sci.* 41 (2006) 4335.

[33] http://webbook.nist.gov/cgi/cbook.cgi?Name=ethyleneglycol&Units=SI

[34] M. Schindler, W. Joswig, W. B. Baur, *J. Solid State Chem.* 145 (1999) 15.

[35] K.H. Lii, C.H. Li, T.M. Chen, S.L. Wang, *Z. Kristallogr.* 197, 1-2 (1991) 67.

[36] Q.Z. Huang, Y.Q. Feng, Z.H. Meng, H.Z. Shi, *Russian J. Electrochem.* 36, 8 (2010) 572.

[37] P. Nagaraju, N. Lingaiah, P.S.S. Parsad, V. Narayana Kalevaru, A. Martin, *Catal. Comm.* 9 (2008) 2449.

[38] F. Sauvage, E. Quarez, J.-M. Tarascon, E. Baudrin, *Solid State Sci.* 8 (2006) 1215.

[39] W. Massa, O.V. Yakubovich, O.V. Dimitrova, *Solid State Sci.* 4 (2002) 495.

[40] T. Jiang, G. Chen, A. Li, C. Wang, Y. Wei, *J. Alloys Compd.* 478 (2009) 604.

[41] R.K.B. Gover, A. Bryan, P. Burns, J. Barker, *Solid State Ion.* 177 (2006) 1495.

[42] J. –M. Le Meins, M. –P. Crosnier-Lopez, A. Hemon-Ribaud, G. Courbion, *J. Solid State Chem.* 148 (1999) 260.

[43] R. Aiello, G. Giordano, F. Testa, *Impact of zeolites and other porous materials on the new technologies at the beginning of the new millennium*, Elsevier Science B. V. (2002)

# CHAPTER 4
# CONCLUSIONS AND FUTURE WORK

# 4. CONCLUSIONS AND FUTURE WORK

The main objective of this work was to synthesize new microporous and related materials, starting from modification of the well known microporous titanosilicate ETS-4, and a systematic synthesis research of a vanadium phosphate composition which is close related to the synthesis of $Na_3V(OH)(HPO_4)(PO_4)$.

Iron substitute materials have been synthesized by in situ adding iron trichloride in precursor. Iron exchange experiments of ETS-4 were also carried out, with the same iron source. The results have been compared and influence of direct ion substitution has been studied.

The addition of iron trichloride in precursor does not significantly modify the crystallization process of ETS-4 synthesis. Iron substituted ETS-4 samples were successfully prepared under hydrothermal conditions with different amounts of iron being incorporated in ETS-4 framework, giving samples Fe-ETS-4(x) (x=5, 9, 13 and 19). XRD proves that after iron incorporation, no significant structural changes occurred in Fe-ETS-4(x) materials. All spectroscopic results present no profound alterations. By comparison of the results of the in situ synthesized and ion exchanged samples, $^{29}$Si MAS NMR results suggest that Fe is not located in the pores of ETS-4 as a charge compensator. However, the location of Fe ions in ETS-4 framework is still an open question. The variability of Fe with different radii in various coordination and spin state makes the system complicated. In future, (1) Mossbauer spectroscopic studies can be carried out to help in the detailed description of the iron substitution in ETS-4, namely the location of Fe in the framework; (2) the properties of Fe-ETS-4(x) materials, such as adsorption, ion exchange ability, catalytic ability, can be explored.

On the other hand, spectroscopic results of ion exchanged samples are clearly different to those of parent material although their XRD patterns are very similar. The thermal stability of iron exchanged sample is much low. As we know that iron only replaces the exchangeable Na cations of ETS-4 in this experiment,

the spectroscopic results strongly suggest that iron is not in pore of in situ synthesized Fe-ETS-4(x) samples.

In the study of vanadium phosphate synthesis, several different parameters were varied in order to evaluate its influence on the final product., like the time, addition of organic additives, different solvents and different heating processes.

The starting system for these experiments was with a molar composition of $1VO_2$-$4.4P_2O_5$-$4.4Na_2O$-$236.8H_2O$, hydrothermally synthesized for 7 days at 170 ºC. The product was a known crystalline phase, $Na(VO)(PO_4)$.

Addition of two organic compounds, maleic acid or urea, was tested. The presence of these additives influences the formation of vanadium phosphate phases, producing two different crystalline materials which cannot be identified as single phase or mixed phases from XRD database. As future work, studies will be carried out to confirm phase purity and to determine their structures.

The product also depends on the synthesis time. Synthesis of vanadium phosphates with maleic acid were carried out during different periods of time (5 hours, 10 hours, 1 to 7 days, 2 and 3 weeks). Initial synthesis periods form different compounds, between 10 hours and 7 days the crystal phase is stable, while for longer synthesis times structural changes occur again. The sample synthesized for 2 weeks resulted in a crystalline product with the structure very similar to the phase, $Na_3V_2O_2(PO_4)_2F$. The synthesis parameters here are totally different to that of $Na_3V_2O_2(PO_4)_2F$. It would be very interesting, in the future, to evaluate the influence of synthesis time on the system with addition of urea. The possible application of this material as cathode materials for batteries will also be interesting work in future.

Experiments where water was substituted by ethylene glycol or eutectic mixtures were also carried out. Syntheses with total absence of water resulted in low crystalline product with few peaks at high 2θ in the XRD. On the other hand, synthesis with both water and eutectic mixture resulted in the formation of a known

phase $Na_3VO(PO_4)(HPO_4)$. This composition is very similar to the mentioned one [23]. However, their structures and vanadium valence are totally different.

Microwave heating assisted synthesis was used as an alternative method to conventional (hydrothermal) synthesis. Crystalline products were obtained for short periods of synthesis, proving the efficiency of microwave heating.

It should be noted that this system shows great versatility. Every synthesis parameter that was altered may modify the crystallization process and thus the products. In future, other parameters can still be studied for this system, like temperature, careful control of pH, use of other type of solvents, for example. It is clear by this work that synthesis of new materials from known compositions is still possible. All the known phases obtained in this work contain V(IV), indicating that the reduction of vanadium using these organic additives is not efficient.